TABLE OF CONTENTS

1. INTRODUCTION
2. CHANGE LOG
3. LINKS TO RELEVANT INFORMATION IN THE ONLINE NSSDC INFORMATION SYSTEM
    a. URL to S/C “Remarks” field
    b. URL to S/C “Materials” field
    c. URL to Experiment “Remarks” field
    d. URL to Experiment “Materials” field
    e. URL to Data Set “Remarks” field
    f. URL to Data Set “Materials” field
    g. Items e and f for additional data sets from this experiment, if needed
    h. Items c thru g for additional experiments from this spacecraft, if needed
    i. Items a thru h for additional spacecraft, if needed
4. CATALOG MATERIALS.

1. Introduction:

The documentation for this data set was originally on paper kept in NSSDC's Data Set Catalogs (DSCs). The offline tape datasets have now been migrated from the original magnetic tape to magnetic disk (starting in mid-2004). Accordingly, statements in the format descriptions that address such tape relevant factors as blocking and but density are no longer applicable. The paper documentation in the Data Set Catalogs have been scanned and made into digital images of the pages, the collected into a single PDF file for each Data Set Catalog.

The inventory information in these DSCs is current as of July 1, 2004. But this inventory information is now no longer maintained in the DSCs, but is now managed in the inventory part of the NSSDC information system, and the user should go to that interface (JIN) if further information existing in the DSCs is now not needed for locating data files, but we did not go to the trouble of removing that inventory information.

2. CHANGE LOG

Version	Date	Person	Page	Description of Change
01				

3. LINKS TO RELEVANT INFORMATION IN THE ONLINE NSSDC INFORMATION SYSTEM:
[NOTE: ANY OF THE INFORMATION FIELDS MIGHT BE BLANK.]
[THE "MATERIALS FOR DISTRIBUTION" FIELD IS HERE CALLED JUST "MATERIALS"]

"Remarks" for spacecraft SCNAME1":
http://nssdc.gsfc.nasa.gov/database/MasterCatalog?sc=1977-102A--remark--

"Materials" for spacecraft SCNAME1":
http://nssdc.gsfc.nasa.gov/database/MasterCatalog?sc=1977-102A--mat--

"Remarks" for SCNAME1 experiment EXNAME1:
http://nssdc.gsfc.nasa.gov/database/MasterCatalog?sc=1977-102A&ex=09--remark--

"Materials" for SCNAME experiment EXNAME1:
http://nssdc.gsfc.nasa.gov/database/MasterCatalog?sc=1977-102&ex=09--mat--

"Remarks" for EXNAME1 data set DSNAME1:
http://nssdc.gsfc.nasa.gov/database/MasterCatalog?ds=SPHE-00677--remark--

"Materials" for EXNAME1 data set DSNAME1:
http://nssdc.gsfc.nasa.gov/database/MasterCatalog?ds=SPHE-00677--mat--

"Remarks" for EXNAME1 data set DSNAME2:
http://nssdc.gsfc.nasa,gov/database/MasterCatalog?ds=SPHE-00677--remark--

"Materials" for EXNAME1 data set DSNAME2:
http://nssdc.gsfc.nasa.gov/database/MasterCatalog?ds=SPHE-00677--mat--

"Remarks" for EXNAME1 data set DSNAME3:

"Materials" for EXNAME1 data set DSNAME3:

"Remarks" for SCNAME1 experiment EXNAME2:

"Materials" for SCNAME1 experiment EXNAME2:

"Remarks" for EXNAME2 data set DSNAME1:
"Materials" for EXNAME2 data set DSNAME1:

"Remarks" for EXNAME2 data set DSNAME2:
"Materials" for EXNAME2 data set DSNAME2:

“Remarks” for spacecraft SCNAME2”:
http://nssdc.gsfc.nasa.gov/database/MaterCatalog?sc=1978-079A--??--

“Materials” for spacecraft SCNAME2:
http://nssdc.gsfc.nasa.gov/database/MaterCatalog?sc=1978-079A--??--

“Remarks” for SCNAME2 experiment EXNAME1:
http://nssdc.gsfc.nasa.gov/database/MaterCatalog?sc=1978-079A&ex=03--??--

“Materials” for SCNAME2 experiment EXNAME1”
http://nssdc.gsfc.nasa.gov/database/MasterCatalog?sc=1978-079A&ex=03--??--

“Remarks” for EXNAME1 data set DSNAME1:
http://nssdc.gsfc.nasa.gov/database/MasterCatalog?ds=SPHE--00011--remark--

“Materials” for EXNAME1 data set DSNAME1:
http://nssdc.gsfc.nasa.gov/database/MasterCatalog?ds=SPHE--00011--remark--

“Remarks” for EXNAME1 data set DSNAME2:
http://nssdc.gsfc.nasa.gov/database/MasterCatalog?ds=SPHE-00014--remark--

“Materials” for EXNAME1 data set DSNAME2:
http://nssdc.gsfc.nasa.gov/database/MasterCatalog?ds=SPHE-00014--remark--

“Remarks” for EXNAME1 data set DSNAME3:

“Materials” for EXNAME1 data set DSNAME3:

“Remarks” for SCNAME2 experiment EXNAME2:

“Materials” for SCNAME2 experiment EXNAME2:

“Remarks” for EXNAME2 data set DSNAME1:

“Materials” for EXNAME2 data set DSNAME1:

“Remarks” for EXNAME2 data set DSNAME2:

“Materials” for EXNAME2 data set DSNAME2:

“Remarks” for data set DSNAME3:

“Materials” for EXNAME data set DSNAME3:

“Remarks” for SCNAME2 experiment EXNAME3:

“Materials” for SCNAME2 experiment EXNAME3:

“Remarks” for EXNAME3 data set DSNAME1:

“Materials” for EXNAME3 data set DSNAME1:

“Remarks” for EXNAME3 data set DSNAME2:

“Materials” for EXNAME3 data set DSNAME2:

=-=-= -
=-=-= -

ALTERNATE OPTION:

For SCNAME2:

“Remarks” for EXNAME1 data set DSNAME2:

http://nssdc.gsfc.nasa.gov/database/MasterCatalog?ds=SPHE-00014--remark--

“Materials” for EXNAME1 data set DSNAME2:

http://nssdc.gsfc.nasa.gov/database/MasterCatalog?ds=SPHE-00014--mat--

can be shown as

“Remarks” for EXNAME1 data set DSNAME2:

http://nssdc.gsfc.nasa.gov/database/MasterCatalog?ds=78-079A-03C--remark--

“Materials” for EXNAME1 data set DSNAME2:

http://nssdc.gsfc.nasa.gov/database/MasterCatalog?ds=78-079A-03C--mat--

=-=-= -
=-=-= -

4. CATALOG MATERIALS:

DATA SET CATALOG # 14

Explorer 21, Retarding potential analyzer

64-060A-01A 1 tape

IMP-B

ELECTRON 1, N, V, PLUS ORBIT

64-060A-01A

THIS DATA SET HAS BEEN RESTORED. THERE WAS ORIGINALLY ONE 7-TRACK, 800 BPI TAPE, WRITTEN IN BCD. THERE IS ONE RESTORED TAPE, WRITTEN IN ASCII. THE DR TAPE IS A 3480 CARTRIDGE AND THE DS TAPE IS 9-TRACK, 6250 BPI. THE ORIGINAL TAPE WAS CREATED ON AN IBM 7094 COMPUTER AND THE RESTORED TAPE WAS CREATED ON AN IBM 9021 COMPUTER. THE DR AND DS NUMBER ALONG WITH THE CORRESPONDING D NUMBER AND THE TIME SPAN IS AS FOLLOWS:

DR#	DS#	D#	FILES	TIME SPAN
DR005357	DS005357	D001563	1	10/04/64 - 04/04/65

64-060A-01A
IMP-2
Explorer 21, Retarding Potential Analyzer

800 BPI, 7-track, BCD, 1 file, IBM 7094

D#	C#	START	STOP
D-01563	C-01052	10/[redacted]/64 04	04/[redacted]/65 05

SPACE RESEARCH VII - NORTH-HOLLAND PUBLISHING COMPANY, AMSTERDAM

THERMAL PLASMA MEASUREMENTS WITHIN THE MAGNETOSPHERE

G. P. SERBU and E. J. R. MAIER
Laboratory for Space Sciences, NASA-Goddard Space Flight Center, Greenbelt, Maryland, USA

Abstract. It has been observed that both the ion and electron components of the plasma present within the magnetosphere exhibit, at most times, a Maxwell-Boltzmann energy distribution. The temperature of the electron gas increases by a factor of about 10 from above the ionosphere to an altitude of 2.5×10^4 km ($5R_E$ geocentric). Over this same region, the density decreases to a minimum of about 50 cm^{-3}. Less pronounced variations of temperature and density with radial distance are noted beyond $5R_E$.

The simultaneous observation of ion and electron density profiles provides verification of charge neutrality over vertical dimensions of the order of kilometers.

Резюме: Обнаружено, что в магнитосфере распределение как ионной, так и электронной компонент плазмы по энергиям в большинстве случаев подчиняется закону Максвелла-Больцмана.

В пространстве от ионосферы до высот $2,5 \times 10^4$ км (5 радиусов Земли) температура электронного газа возрастает примерно в 10 раз. Концентрация в той же самой области уменьшается до минимума примерно 50 $см^{-3}$. На расстояниях более 5 R_3 отмечены менее четкие изменения температуры и плотности.

Синхронные наблюдения профилей ионной и электронной концентрации подтверждали предположение о суммарной нейтральности заряда в слоях с толщиной более километра.

1. INTRODUCTION

The satellite IMP-II was launched on 4 October 1964 into an elliptical orbit with a period of 36 hours. The initial perigee was 200 km and the apogee was 95 000 km (15.9R_E geocentric).

Fig. 1 is a polar plot of the IMP-II orbit as seen in geographic latitude and earth radii (R_E) coordinates. At launch the apogee was 20° below the ecliptic plane, with the sun-earth payload angle (LSEP) of 11°. This orbit has offered a good opportunity to investigate the magnetosphere on the day-side of earth near the equatorial plane.

On-board IMP-II was a retarding potential analyzer, which measured the integral spectrum of ions and electrons in the energy interval from 0 to 45 eV. The details of this experiment have been discussed elsewhere [1]. Briefly stated, the experiment consists of performing a measurement of the collector currents as a function of retarding potentials. The retarding po-

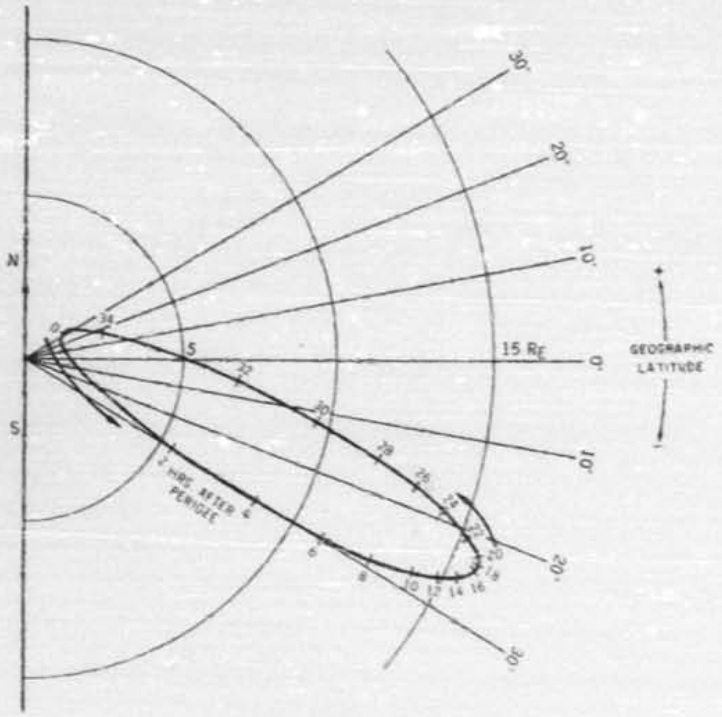

Fig. 1. A view of the latitudinal excursion of the IMP-H spacecraft. IMP-H was launched with the line of apsides extending toward the sun, but inclined about -20° to the ecliptic.

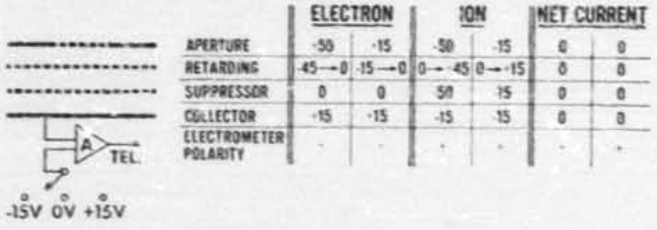

	ELECTRON		ION		NET CURRENT	
APERTURE	-50	-15	-50	-15	0	0
RETARDING	-45→0	-15→0	0→-45	0→-15	0	0
SUPPRESSOR	0	0	50	15	0	0
COLLECTOR	-15	-15	-15	-15	0	0
ELECTROMETER POLARITY	-	-	+	+	-	+

Fig. 2. Schematic representation of the sensor and the experiment voltage program.

tentials used in the measurement are programmed as indicated in fig. 2. The voltage program defines the electron, ion, and net current modes. The electrometer polarity is programmed to give an analog output from 0 to 5 V for negative currents during the electron mode. The electrometer polarity is then reversed in order to measure only positive currents during the ion mode. The effective aperture area of the Faraday cup sensor is 5 cm^2. Particles within an acceptance cone of 170° are accelerated through the aperture and subsequently collected. Photoemission currents from the collector have been successfully suppressed during the electron mode and the 45 V ion mode. Photoemission currents from the suppressor grid can, however, reach the collector and must be accounted for in the analysis.

2. RESULTS

In fig. 3 are plotted two retardation curves obtained on 27 March 1965 while IMP-II was in the nightside magnetosphere on an inbound orbit at a distance between 3.1 and 3.4 R_E. Shown on the left is the negative current response plotted on a log scale as a function of the retarding potential in

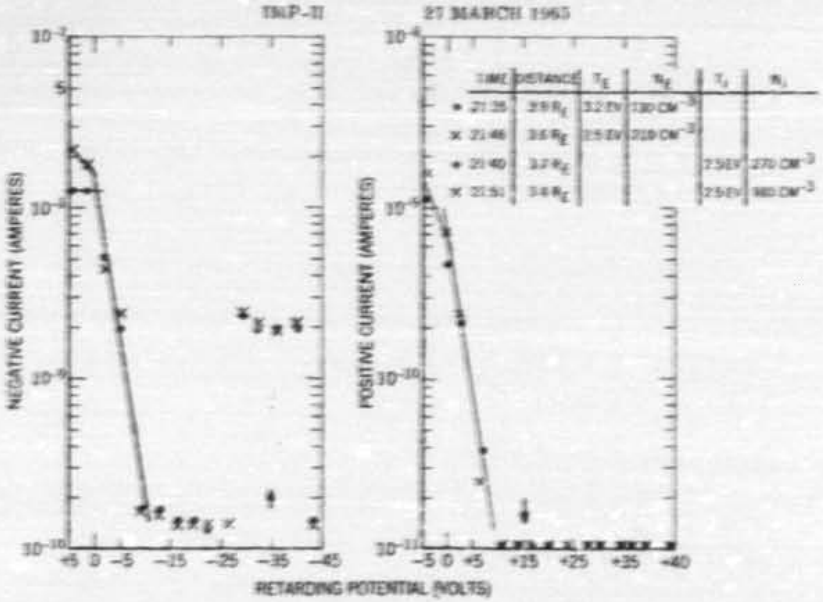

Fig. 3. Sample plots of negative and positive current response as a function of retardation voltage. This data was obtained while IMP-II was on an inbound orbit in the nightside magnetosphere.

volts in the interval from +5 to -45 V. The dots and crosses represent two individual curves which were obtained sequentially within 11 min of each other, during this time interval the satellite traversed $0.3R_E$. The arrow in the figure at -35 V indicates that at this time the plane containing the sun-payload vector was normal to the sensor. The measurements made to within ±85° of the sun contain photoemission currents from the suppressor grid and a correction for this current component should be made on the five data points, symmetric about the sun vector arrow.

The wave form of the current response as a function of retarding potential in the interval from +5 to -10 V can be analyzed in accordance with the Langmuir probe theory for the collection of diffusive currents, which are due to a plasma component having a Maxwell-Bolizmann distribution of velocities. Using this analysis procedure, the electron temperature as measured from the slop of the curve is 3.2 ± 0.2 eV at $3.9R_E$ and 2.5 ± 0.2 eV at $3.6R_E$.

We have observed, in the dayside magnetosphere, on selected days [1] that a well ordered electron temperature structure is present independent of the LSEP angle. For example, in the region from 2 to $5R_E$ the electron temperature increases from 0.3 eV at $2R_E$ to 1.6 eV at $5R_E$. The temperature increase over this region as a function of radial distance can be expressed as $T_e \propto R_E^{+1.9}$. A less pronounced temperature increase is noted at distances beyond $5R_E$.

The data for 27 March 1965 was obtained in the nightside magnetosphere, LSEP ~ 190°. These nightside electron temperature values are about a factor of 3 higher than the corresponding values taken from the dayside temperature profile. Whether spatial or temporal variations are involved cannot be resolved on the basis of these isolated temperature measurements. The 27 March 1965 data (figs. 3 and 4) have been selected to illustrate in detail how electron and ion curves are analyzed; we will be discussing additional data obtained in the dayside magnetosphere.

From the inflection near zero volts of the electron retardation curve in fig. 3 we measure the satellite to plasma potential to be 0 ± 0.5 V. At attractive potentials, i.e., to the left of 0 V, the curve exhibits electron current saturation. Using the measured electron temperature in conjunction with the value of the current at the satellite potential we obtain an electron density of 130 electrons cm^{-3} at $3.9R_E$ and 210 cm^{-3} at $3.6R_E$.

The righthand side of fig. 3 shows the measured positive current plotted on a log scale as a function of the retardation voltage. The wave form of the ion current also exhibits a Maxwell-Boltzmann distribution and so Langmuir probe analysis can be used to determine the ion temperature and density. Since the positive current is retarded almost two orders of magnitude as the retarding voltage is changed from -5 to +7 V, we can measure the slope of the line as drawn through these data points in order to obtain the ion temperature. From this measurement we obtain a value of 2.5 ± 0.5 eV. Assuming that the predominant ion at this altitude ($3.9R_E$) is H^+, we compute the most probable ion velocity to be about 30 km/sec for a 2.5 eV temperature, at $4R_E$ where the satellite velocity is 4 km/sec. Since at this altitude

the ion velocity is much larger than the satellite velocity, no corrections for the sensor orientation with respect to the velocity vector [2] need to be made.

It is evident in the figure that an inflection in the ion curves occurs at about zero volts, the -5 V data point is thus in the ion current saturation region. It is not readily evident when examining the curves at precisely what voltage current saturation occurs; obviously, there is an inflection between -5 and 0 V but the shape of the curve in this interval is not known. Since the saturation point occurs at the satellite potential, its value can be determined with accuracy from the negative current measurement and used to obtain the value of the ion current at saturation. Knowing the value of the ion current at saturation, and the measured ion temperature, we compute ion densities of 270 cm^{-3} at 3.7R_E and 380 cm^{-3} at 3.4R_E.

In computing densities we assign an augmentation factor of 4 to the entrance aperture; this is due to the attractive potential of the aperture. For a more detailed discussion of the augmentation factor, the interested reader is referred to our previous paper [1].

In the legend of fig. 3, we have tabulated the electron and ion densities (N_e, N_i) and the electron and ion temperatures (T_e, T_i). Good agreement is

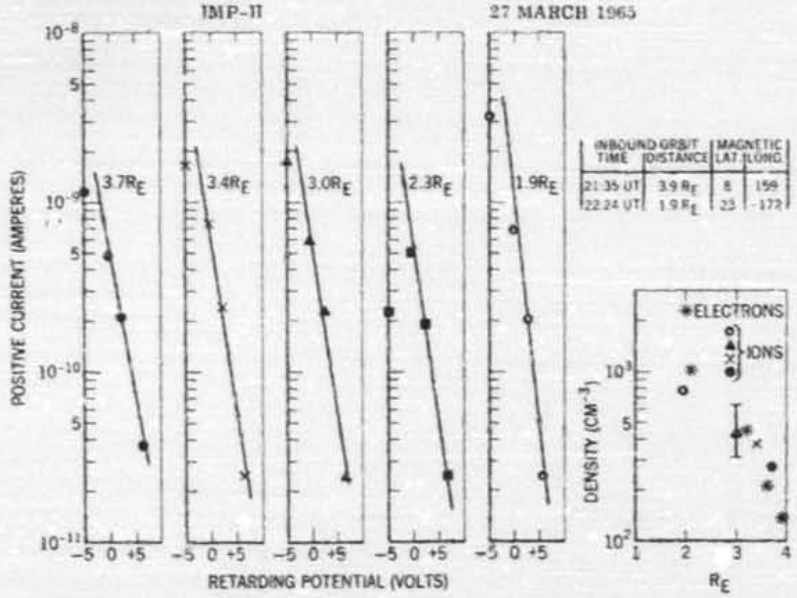

Fig. 4. Five consecutive ion retardation curves are plotted for the inbound orbit of 27 March 1965. The ion density computed from these curves is plotted along with the electron density as a function of geocentric distance.

noted between the measured electron and ion temperatures. The ion density is, within a factor of two, in agreement with the electron density. The factor of two discrepancy is due in part to the previously discussed errors associated with the exact value of the ion current at saturation. Thus, within the limits of the measurement we have determined that the plasma is neutral, at a temperature of about 3.0 eV, and that the spacecraft potential with respect to the plasma is near zero volts.

On this same inbound orbit of 27 March 1965, we have obtained a series of measurements which illustrate how a detailed density profile can be obtained. In fig. 4, we plot five separate ion retardation curves. For reasons of space, we do not show the data beyond +7 V of retardation since they are all similar to the previously shown curves. In the legend, we note that from 2135 UT to 2224 UT the satellite was inbound from 3.9 to $1.9R_E$; the trajectory was near the magnetic equator and northbound. From the electron curves, not shown here, we have determined that for this time interval the satellite potential is 0.5 ± 0.25 V. The previously discussed analysis procedure has been used for each of the curves to obtain a detailed density profile in the nightside magnetosphere region from 3.7 to $1.9R_E$. Note that for the curve marked $2.3R_E$ the data point at -5 V is a factor of ten lower than expected, thus no specific value of density at this radial distance can be obtained; however, the remaining portion of that curve is in general agreement with the preceding and subsequent curves.

The results of our density measurements are plotted in the lower right-hand corner of fig. 4 on a log scale as a function of the radial distance. Included in the plot of density versus R_E are values of electron density (asterisk symbol) and values of ion density. The error bar for the ion density is taken to be a factor of 2, whereas the electron density error bar is less than 15%. It is seen that within the limits of the error bar, the values of ion and electron densities are equal, and thus the measurement indicates a neutral plasma with a density of the order of 10^3 cm^{-3} at $2R_E$ which falls off according to a power law of the radial distance.

In fig. 5, we plot the measured density and temperature profiles for both ions and electrons, obtained within the dayside magnetosphere for the two successive inbound orbits of 28 and 30 October 1964. These two orbits occurred at a sun-earth-payload angle (LSEP) of 38°, thus they are representative of the dayside magnetosphere. Log-log scales have been used to plot the particle density cm^{-3}, and temperature (eV) as a function of geocentric distance R_E. In the figure the crosses represent the ion data and the open circles are for the electron data. The average fall-off rate of the density profile may be approximated by a R_E^{-4} relationship. Spatial deviations from a smooth fall-off rate are noted; however, there is no evidence for a large drop or "KNEE" in the density profile, as has been reported by Carpenter [3].

Slish [4] has recently reported the results of an antenna impedance measurement associated with cosmic noise observations by an experiment on the spacecraft Zond II, launched November 1964. Two independent observations are presented. A peak attributed to electron plasma resonance

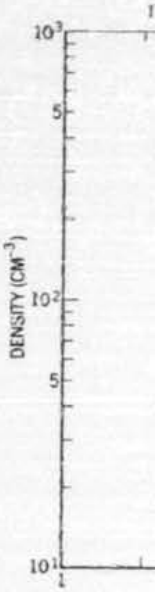

Fig. 5. Electron and i
tric distance. These

was observed in the
observation yields
servation is an anal
ma frequency in ter
tion resistance of t
dence $N_e = 1.3 \times 10$
general radial depe
$6R_E$ are in agreem

Obayashi [5] has
related transmitter
electron density in
cal density at local
geocentric distance
vember 1964 at 110
10^3 electrons cm^{-3}

In fig. 5, the ten
geocentric distance
crease with distanc

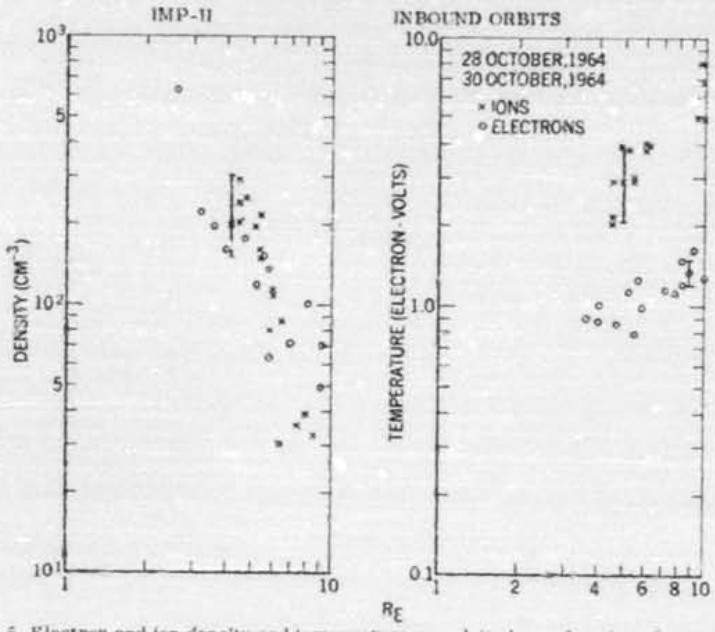

Fig. 5. Electron and ion density and temperature are plotted as a function of geocentric distance. These data were obtained while IMP-II was near the ecliptic plane in the dayside magnetosphere.

was observed in the 210 kc/s receiver response at $4R_E$ geocentric. This observation yields a local density of 550 electrons cm^{-3}. The second observation is an analysis of the receiver response to a signal above the plasma frequency in terms of the effect of the local plasma density on the radiation resistance of the antenna. Interpreted in this manner, a radial dependence $N_e = 1.3 \times 10^5 (R/R_0)^{-4}$ valid from 4 to $7R_E$ is obtained. Both the general radial dependence and the specific value of 100 electrons cm^{-3} at $6R_E$ are in agreement with our results.

Obayashi [5] has used the differential Doppler shift of the harmonically related transmitters (40 and 360 Mc/s) on OGO-A to determine the local electron density in the vicinity of the spacecraft. He obtains an average local density at local noon on 16 November 1964, of 1 to 2×10^3 cm^{-3} at a geocentric distance of $3.2R_E$. The IMP-II satellite was at $3.3R_E$ on 16 November 1964 at 1103 UT; the density value as measured by us was 1.04×10^3 electrons cm^{-3}.

In fig. 5, the temperature profiles for ions and electrons as a function of geocentric distance are in general agreement in the rate of temperature increase with distance; however, we note that the ion temperature is higher

than the electron temperature, taking into account the appropriate errors. It appears that near the magnetopause, approximately $10R_E$, the ratio of ion-to-electron temperature is higher than that at $5R_E$. We suggest that this preliminary observation might possibly be interpreted as follows: In the magnetosheath, solar wind energy is transferred to the thermal ions raising their temperature well above that of the thermal electrons. The electron temperatures in the magnetosheath have been observed to be between 1 and 3 eV [1]. Theoretical treatments of the detailed process involved in thermalization of the solar wind have been presented by Scarf et al. [6] who suggested that solar wind ions lose speed in the sub-solar magnetosheath resulting in the generation of ion-waves and that the electric fields associated with the waves allow fast diffusion of plasma into the magnetosphere. Eviatar [7] finds that the interaction with electron plasma oscillations are effective in scattering super-thermal electrons and that ion waves are the dominant mechanism for the diffusion of sub-thermal (1 eV) electrons across the magnetopause.

It appears that within the magnetosphere, the ion temperature decreases from its relative high value in the magnetosheath, due to heat transfer to the electrons. Such a mechanism could explain the thermal gradients in the magnetosphere, and account for the fact that the ion-to-electron temperature ratio decreases with distance from the magnetopause.

3. CONCLUSIONS

The results of successive and continuous measurements of positive and negative retardation currents within the magnetosphere have been presented. Our interpretation of these measurements are summarized as follows:

1. Electrons and ions have a Maxwell-Boltzmann distribution of velocities in the thermal energy range of the order of eV; these particles constitute a neutral plasma.

2. Within $5R_E$ in the magnetosphere we observe a temperature profile which increases approximately as the square of the radial distance, while the density profile exhibits a decay that can be approximated by the inverse third to fourth power of the radial distance.

3. Our measurements of particle density do not indicate a whistler "KNEE" phenomenon. In fact, we observe 10 to 50 times as large a density beyond the "KNEE" as has been reported from whistler results.

REFERENCES

[1] G. P. Serbu, E. J. R. Maier, J. Geophys. Res. 71 (1966).
[2] E. C. Whipple, Goddard Space Flight Center Report X-615-65-296 (1965).
[3] D. L. Carpenter, J. Geophys. Res. 71 (1966).
[4] V. I. Slish, Cosmic research, vol. III.
[5] T. Obayashi, Rep. Ionos. Space Res. Japan, 19 (1965).
[6] F. L. Scarf, W. Bernstein and R. W. Fredericks, J. Geophys. Res. 70 (1965).
[7] A. Eviatar, J. Geophys. Res. 71 (1966).

JOURNAL OF GEOPHYSICAL RESEARCH VOL. 71, NO. 15 AUGUST 1, 1966

Low-Energy Electrons Measured on IMP 2

G. P. SERBU AND E. J. R. MAIER

Laboratory for Space Sciences
Goddard Space Flight Center, Greenbelt, Maryland

The integral spectrum for low-energy electrons has been measured with detailed definition of temperature and number density throughout the IMP 2 orbit. Electrons are found to have a Maxwellian distribution at energies below 2.0 ev with a component of higher energy. The electron temperature typically increases from above the ionosphere as the square of the radial distance, whereas the number density decreases approximately as the inverse cube of the distance out to 5 R_E. From 5 to 15.9 R_E (apogee) the temperature remains between 1.9 and 2.0 ev, and the number density remains between 25 and 50 electrons/cm^3. It is verified that the observed positive ion density of 25–50 cm^{-3} is in agreement with the number of electrons observed per unit volume in the solar wind region. The location of the magnetopause is not evident in the low-energy electrons; however, a small temperature increase is noted at the shock boundary. An intensity increase is noted in the energetic electron component in the magnetosheath. Data for a six-month period covering a 180° sector of the earth's environment is reported on.

These observations constitute the first integral measurements in the solar wind region of charged particle spectra in the energy range 0–45 ev. Our observations of the number density are in disagreement with presently accepted solar wind theory but are not inconsistent with previous measurements of the streaming ions.

1. INTRODUCTION

The Interplanetary Monitoring Platform, IMP 2, or Explorer 21, was launched from the Atlantic Missile Range, Cape Kennedy, Florida, on October 4, 1964, at 03:52 UT. On board both this spacecraft and IMP 1 were essentially identical retarding potential analyzer experiments. Table 1 presents the most significant initial orbital characteristics of the two missions. From the data in the table it is clear that while IMP 2 does not penetrate into the solar wind region to the extent IMP 1 has done, the IMP 2 mapping of the magnetosphere is more detailed than that of IMP 1.

It is the purpose of this paper to present and discuss some of the results of the Retarding Potential Analyzer experiment on board the IMP 2 spacecraft. The primary objective of this experiment was to measure the electron and ion densities and energies as a function of orbital position. The integral spectrum of charged particle energies was obtained in two separate ranges: (1) a high-resolution thermal range from 0 to 15 volts and (2) a low-resolution range from 0 to 45 volts. Thus far, the electron current voltage characteristics have been analyzed for a period of 150 days in orbit; some preliminary results of this analysis are presented at this time. Future publications concerning this IMP 2 experiment will treat the ion data results obtained in this same time interval.

This paper considers the experimental arrangement including the geometric properties of the sensor, the procedure for data acquisition and analysis, and a discussion of some experimental results.

The observations of electron density distribution and electron temperature profiles obtained within the magnetosphere are presented. The locations of the magnetopause and shock front as determined from our data are given for sun-earth-satellite angles from 11° to 90°. A few observations made in the solar wind region are also presented, and in addition measured values of satellite-to-plasma potentials are given.

2. EXPERIMENTAL ARRANGEMENT

The sensor, shown schematically in Figure 1, is a Faraday cup of planar geometry so designed as to measure the integral spectrum in the thermal range of energies for both ions and electrons.

TABLE 1.

IMP Launch	Orbital Period, hrs	Inclination	Eccentricity	Apogee, km	Perigee, km	Spin, rpm	Spin Axis Sun Angle
02:30 UT, 11/27/63	93.5	33.33°	0.937	197616	192	22.3	111°
03:52 UT, 10/4/64	34.07	33.53°	0.878	95016	200	14.2	131°

The ambient plasma can be considered as incident on the spacecraft at the sensor at the vector sum of the plasma streaming velocity and the spacecraft velocity. The spacecraft velocity is at all times small compared to the velocity of even at 0.1 ev (1170°K) electron and thus can be ignored in the analysis of the electron data. When the spacecraft is near perigee, its velocity is comparable to ion velocities, and it is necessary to include spacecraft attitude and velocity in the reduction of the ion data. The aperture is a hole of 5-cm² area over which is stretched a fine wire mesh having an optical transparency of 95%. Surrounding the aperture is a tungsten surface of 35-cm² area, which is electrically connected to the aperture grid.

The accompanying table in Figure 1 shows the series of voltages that are programmed on the various trap elements to define the six modes of operation. For example, the electron spectrum is obtained as follows: a +45-volt aperture potential will effectively separate out from the entering plasma those ions with energies below 45 ev. The negative voltage programmed on the retarding grid sequentially and in synchronism with the telemetry system then yields the integral spectrum of electron current as a function of retarding potential in the interval from +5 to −45 volts. The suppressor grid is used to suppress secondary electrons emitted from the collector. In the electron mode the collector is maintained positive to insure collection of all electrons that pass through the retarding and suppressor grids. The retarding potential is programmed in fifteen discrete voltage increments from +5 to −45 volts in a period of 5.2 sec. The entire ion, electron, and net current measurement cycle is completed every 648 sec.

Fig. 1. Schematic representation of the sensor and the experiment voltage program.

Examination of the potential on the suppressor illustrates that during the two electron modes of operation and during the low resolution ion mode the photoemission currents from the collector have been suppressed; however, photoelectrons emitted from the suppressor grid itself will reach the collector and register as a negative current component, which varies as a function of the solar aspect. The magnitude of this current being directly proportional to the area of the grid wires is expected to be of the order of 10^{-8} amp. In the analysis of the electron current, use is made of the spacecraft optical aspect sensor to compute the precise times at which the sun vector lies in the plane defined by the spin axis and the sensor normal. Data obtained during the time when the sun is within ±70° of the trap normal are eliminated from the analysis. In practice this means that five data points are eliminated from the total spectrum of 15 data points. Owing to the fact that the satellite spin rate is not synchronous with the retardation program, the data points dropped in the analysis fortunately do not always fall in the rapidly changing portion of the spectrum. The net effect is that not all current voltage characteristics obtained can subsequently be analyzed to yield electron temperatures and densities. However, the large amounts of data received still allow us to make a meaningful measurement at increments of 0.1 R_e along nearly the entire orbit, the exception being at altitudes below 10,000 km where the satellite velocity and orientation are changing

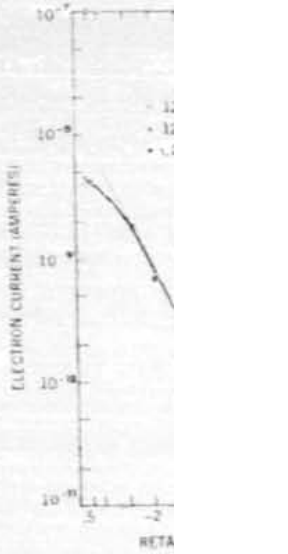

Fig. 2. Sample
tardation curves.
rent is plotted as
tion potential in vo

much too rapidly
required to obtain

The collector c
trometer whose
10^{-8} amp to 1 ×
log output of th
the telemetry sy
volts full scale.
operation, the e
to negative curr
the response is to

Incorporated
internal calibrati
data analysis pr
calibration and
For the first th
trometer gain ch
ing January th
operation was i
favorable sun-s
gradually impro
operation was
significant gain
ing this period.

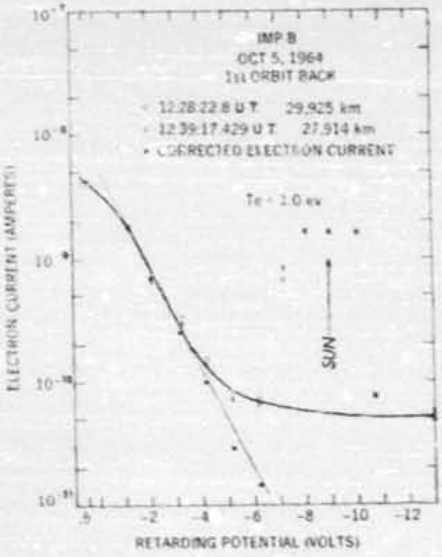

Fig. 2. Sample electron current-voltage retardation curves. The logarithmic negative current is plotted as a function of the linear retardation potential in volts.

much too rapidly in the time interval of 5.2 sec required to obtain one spectrum.

The collector current is measured by an electrometer whose sensitivity ranges from 1×10^{-13} amp to 1×10^{-7} amp full scale. The analog output of the electrometer is presented to the telemetry system as a voltage from 0 to 5 volts full scale. During the electron mode of operation, the electrometer can respond only to negative currents, and during the ion mode the response is to positive currents.

Incorporated within the experiment is an internal calibration capability. One step in the data analysis procedure is to check this internal calibration and make appropriate corrections. For the first three months in orbit, the electrometer gain change was less than 5%. During January and February 1965 the satellite operation was intermittent because of an unfavorable sun-solar paddle aspect angle that gradually improved so that by March full-time operation was again achieved. There were no significant gain changes in the electronics during this period.

3. Data and Analysis

Figure 2 is a sample of the current voltage characteristics obtained with the Retarding Potential Analyzer experiment as flown on IMP 2. Plotted on a logarithmic scale is the negative current as measured by the electrometer as a function of the linear abcissa that is the retarding potential in volts. Two spectrums obtained within 11 minutes of each other on October 5, 1964, are illustrated as the open circles and crosses in Figure 2. In the elapsed time of 11 minutes, the satellite has moved 2011 km at an altitude of approximately 28,000 km; however, the two spectrums are virtually identical in shape and form. Each spectrum is obtained within 5.2 sec, which corresponds to 15-km translational motion, thus illustrating that in this region of the earth's magnetosphere the plasma characteristics are not changing too rapidly. The arrow in the figure marks the precise point during the spectrum at which the sun vector is normal to the trap, thus indicating that the five data points symmetric in time about the sun position contain photoemission currents and that these points should be discarded in the analysis. A smooth curve as shown can be drawn through the remaining 10 data points.

It has been found that the data can be well-fitted by considering the plasma to consist of two components having Maxwellian energy distributions. It should be pointed out that both components are omnidirectional. One, the 'thermal component,' has a mean energy below 4 ev; the second, the so-called 'high-energy component' has a mean energy much higher than 4 ev. Separation of the two components results in the retardation spectrum for the thermal component as illustrated by the solid-dot curve in Figure 2. The 100-to-1 logarithmic decrease in electron current with increasing retarding voltage establishes that the energy distribution of the thermal component is Maxwellian. Note that the high-energy tail is only partially retarded because of the limited range of the sweep voltage in the experiment. This limited retardation does not enable us to distinguish the true nature of the energy distribution of the high-energy component; that is, an equally good fit to the data would be obtained using other functional relationships.

The exponential is used primarily for convenience; its use in the case of the high-energy component does not necessarily imply the existence of thermal equilibrium for that component.

A computer program has been generated to process the satellite telemetry information, convert this to current (I) — voltage (V) characteristics, and eliminate the data points containing a photocurrent component. Analysis of the selected, corrected data points is then carried out by the computer. The analysis consists of performing a least-squares fit by an iterative process to an appropriate combination of exponential distributions, using only the data obtained in the retarding region of the basic I-V curve. The data fit to the computed exponential has typically a fractional root mean deviation in the range from 0.001 to 0.1. The temperatures of the two distributions are then directly obtained as the exponent coefficients of the best-fitted exponentials. In accordance with Langmuir probe theory, the density is computed from the value of the thermal current at the satellite potential and the temperature of the thermal component. In this case, the satellite potential is taken to be the negative value of the sweep voltage at the inflection of the curve.

At times, should the satellite be more negative than 0.5 volts, no inflection is obtained and thus density values cannot be computed. In general, the satellite potential is positive between 0 and +2 volts with respect to the plasma for all parts of the orbit at distances greater than about 2 R_E.

In most cases, the analysis program has worked very well; the only difficulty experienced with this procedure has been for data obtained in the transition region (beyond 10 R_E) where the ratio of the maximum thermal electron current values to the mean of the high-energy component value is less than three to one, thus making it somewhat difficult to meaningfully separate the two individual components.

Throughout much of the spacecraft orbit, the Debye length, and thus the 'sheath thickness,' is in excess of 10 cm. The proper interpretation of the probe characteristic in the unretarded portion of the sweep is extremely complex. Theoretical studies [*Parker*, 1965] assuming idealized, but reasonable, boundary conditions indicate that the enhancement of the effective area over the geometric area may be of the order of a factor 5 to 10. The factor-of-10 enhancement is predicted if the field in the vicinity of the trap is defined by Laplace's equation. This is evidently an upper limit for the enhancement. The presence of a sheath will screen the local field and yield a smaller enhancement factor.

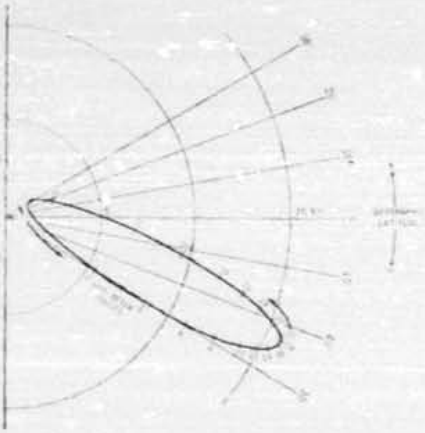

Fig. 3. A view of the latitudinal excursion of the IMP 2 spacecraft. IMP 2 was launched with the line of apsides extending toward the sun, but inclined about −20° to the ecliptic.

Results obtained by programming different potentials on the entrance aperture do not indicate as severe an increase of observed saturation current with applied accelerating potential as is predicted for the idealized geometry. The observation of a nonlinear dependence on accelerating potential is evidence of the above-mentioned screening. Thus the minimum possible effective area is the geometric area of the aperture A_o. The maximum possible effective area is that predicted for zero local charge density; its value is 10 A_o. Applying these two possible values for the area to our observed saturation electron currents yields upper and lower bounds for the electron density. By combining Parker's predicted enhancement factor and the observed effect of different acceleration potentials, we arrive at 4 as the best value for the enhancement. The densities presented are obtained by using 4 A_o as the effective area. From the above

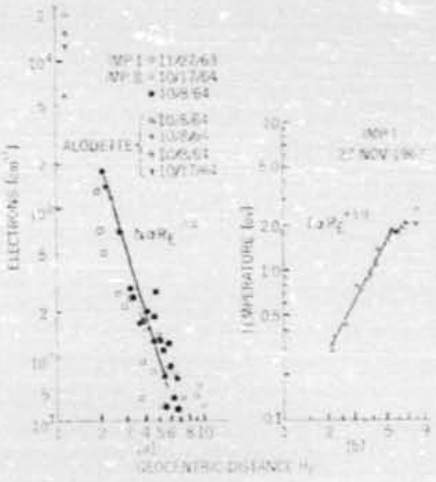

Fig. 4. Plot of the electron density and temperature as a function of geocentric distance. Data obtained from IMP 1 and IMP 2 and the topside sounder satellite, Alouette I, are presented.

considerations it is believed that this augmentation factor is known to within a factor of 2 so that the absolute values of densities may be in error by a factor of 2. It should be emphasized that relative errors are determined by the stability of the electronics, which is of the order of 5%.

4. Results

1. *Magnetosphere.* Figure 3 is a view of the latitudinal excursion of the IMP 2 spacecraft. The satellite passes through the earth's equatorial plane from north to south on the outbound leg of the trajectory. In general, at large distances the satellite is in the southern hemisphere and within 30° of the geographic equator. Closer in than 5 R_E on the inbound trajectory the satellite crosses through the equatorial plane toward its maximum northern latitude of 33.5°. Essentially, then, within the magnetosphere the IMP 2 orbit is near the equatorial plane, and it is useful to compare the data with the whistler profiles taken in the equatorial plane.

Carpenter and Smith [1964] have presented experimental results from whistler observations indicating that in the equatorial plane the electron distribution can be represented in accordance with $N_e \propto R_E^{-3}$ or $N_e \propto R_E^{-4}$, where the electron density N_e is a smooth function of the geocentric distance R_E in earth radii. This relationship exists out to about 5 R_E.

The knee whistlers described by *Carpenter and Smith* [1964] and *Carpenter* [1963, 1966] present a second type of measured electron distribution in which the density suddenly drops a factor of 50 or more at distances varying between 3 and 5 R_E. The knee in the equatorial profile leads them to classify the magnetosphere into two regions: an inner relatively quiet magnetosphere in which particles are in some form of a modified diffusive equilibrium and an outer region having extremely low densities of thermal plasma.

Figure 4a is a plot of the electron density as a function of geocentric distance along the orbit. Included in this plot are data from IMP 1 taken on October 27, 1963 [*Serbu*, 1965, open box points], and data from two orbits of IMP 2 taken on the inbound pass on October 8, 1964, and the outbound pass of October 17, 1964. In the region from 2 to 5 R_E, the density falls off as the -3.4 power of the distance; from 5 to 10 R_E the density is observed to be in the range from 25 to 80 el/cm³. This observation of approximately uniform density from about 5 to

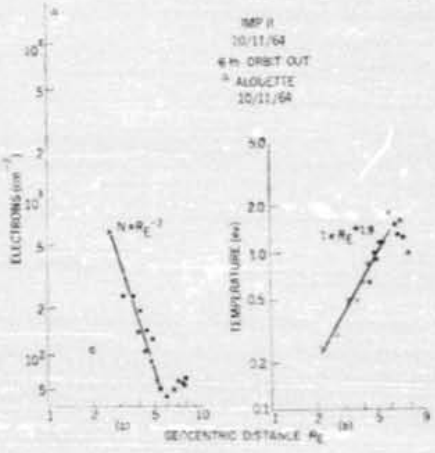

Fig. 5. Electron density and temperature profiles obtained on the 6th outbound orbit of October 11, 1964.

10 R_E has been repeated consistently, and we will subsequently discuss it in detail. It is of interest to note that the IMP 1 and 2 density results have the same general rate of decay with distance; however, the 1963 data seem lower by about a factor of 3. Since the two satellites were in essentially the same region of space, we attribute this difference in measured density value to a temporal variation. Also shown in Figure 4a are four values of electron density at 1000 km, which were computed from topside ionograms obtained by the Alouette 1 satellite near the time of the IMP 2 data observations. Three out of four of the ionogram values compare favorably with extrapolated IMP measurements. An additional comparison with Alouette is presented in Figure 5a. The purpose is to illustrate that the extrapolated IMP measurement, in general, agrees within a factor of 3 with the Alouette value at 1000 km.

The October 11, 1964, data, Figure 5a, illustrates more clearly the shape of an individual profile. Data points closer in than 2 R_E are difficult to obtain because of poor telemetry acquisition and also because the orbital velocity is sufficiently high to cause significant spacecraft motion during the time of one sweep. As can be seen, neither of the density profiles in Figures 4 and 5 indicate a knee-type of falloff in the region from 3 to 5 R_E; in fact, our density at 5 R_E is just about a factor of 10 above that reported by *Angerami and Carpenter* [1966] and by *Taylor et al.* [1965]. *Obayashi* [1965] has used the differential Doppler shift of the harmonically related transmitters (40 and 360 Mc/s) on OGO-A to determine the local electron density at the spacecraft. He obtains an average local density at local noon November 16, 1964, of 1 to 2 $\times$ 10^3 cm^{-3} at a geocentric distance of 3.2 R_E. The IMP 2 satellite was at 3.3 R_E on November 16, 1964, at 11:03 UT; the density value as measured by us was 1.04 $\times$ 10^3 electrons cm^{-3}. These data were obtained about 44 hours after Obayashi's measurement and agree very well with his result.

Slish [1965] has recently reported the results of an antenna-impedance measurement associated with cosmic-noise observations by an experiment on the spacecraft Zond 2 launched November 1964. Two independent observations are presented. A peak attributed to electron plasma resonance is observed in the 210-kc/s receiver response at 4 R_E geocentric. This observation yields a local density of 550 electrons cm^{-3}. The second observation is an analysis of the receiver response to a signal above the plasma frequency in terms of the effect of the local plasma density on the radiation resistance of the antenna. Interpreted in this manner, a radial dependence $n_e = 1.3 \times 10^5 (R/R_e)^{-4}$ valid from 4 to 7 R_E is obtained. Both the general radial dependence and the specific value of 100 electrons cm^{-3} at 6 R_E are in excellent agreement with our result.

In the region of space through which we have noted a smooth falloff rate in the density of electrons, we also observe that the temperature of the low-energy electrons is increasing according to a power law of the geocentric distance. The November 27, 1963, IMP 1 temperature profile is shown in Figure 4b, where we plot the electron temperature as a function of geocentric distance in earth radii on a log-log scale. In the region from 2 to 5 R_E, the electron temperature increases from 0.3 ev at 2 R_E to 1.6 ev at 5 R_E. The accuracy of the IMP temperature measurement is dependent upon the straight-line fit through corrected electron current values, i.e., the solid dots in Figure 2. In general, the fit of these values to a straight line is good over a 100-to-1 range in current amplitude; thus the electron temperature, i.e., the line slope, can be determined to within ± 0.1 ev. The data points in the 2-to-5 R_E region fit rather well to a power law $T_e \propto R_e^{+1.9}$. The October 11, 1964, profile, Figure 5b, is also smoothly increasing with a +1.9 power of the radial distance. At distances from 5 to 10 R_E the electron temperature remains in the range from 1 to 3 ev. Thus, we see that within the 5-R_E distance the pressure of the electron gas as derived from these profiles of temperature and density is inversely proportional to the distance; from 5 to 15.9 R_E (apogee) the pressure remains approximately constant.

To organize the large volume of data obtained from IMP 2, we have set up criteria whereby the data is separated into two broad categories on the basis of the observed plasma parameters:

1. A 'quiet' condition exists when we observe a smooth temperature profile in the region below 5 R_E accompanied by a high ratio of the thermal electron current to the more energetic

TABLE 2. Parameters m and n, Which Are Descriptive of the Temperature and Density Profiles Obtained within a 190° Sector of the Earth-Sun Line

Date	Time at 2 R_E, UT	Time at 5 R_E, UT	Magnetic Latitude, deg		$N \propto L^{-n}(n)$	$T \propto L^{-m}(m)$	Sun-Earth-Satellite Angle, deg
			2 R_E	5 R_E			
Oct. 22, 1964	23:00	0:20	−25	−45	−2.1	1.4	30
Oct. 24, 1964	9:50	11:00	−15	−22	−2.5	2.1	32
Oct. 27, 1964	7:00	8:20	−7	−23	−3.3	1.5	35
Oct. 31, 1964	14:00	12:50	+20	−3	−1.6	1.3	39
Nov. 4, 1964	22:10	21:00	+30	+3	−1.9	1.5	41
Nov. 6, 1964	9:50	11:00	−19	−22	−2.3	3.9	43
Nov. 17, 1964	23:00	0:10	−23	−42	−2.8	2.1	56
March 16, 1965	9:50	11:00	−39	−41	−3.1	1.6	174
April 4, 1965	03:50	02:30	+28	+3	−2.8	1.9	193

electron current. Within the magnetosphere this ratio is generally 10 to 1 or more on the quiet transits; through the magnetosheath the ratio is generally less than 5. Data presented in Figures 4 and 5 are representative of quiet conditions.

2. A 'disturbed' condition is typified by the fact that the electron temperature reaches values of 1–3 ev at distances closer in than 5 R_E, and the high-energy component is large so that the ratio of thermal to more energetic electrons is not greater than 5 to 1. In Table 2 are presented the values of parameters descriptive of the temperature and density profiles for 9 orbits obtained during quiet transits within a 190° sector of the earth-sun line; the orbit precessed through this 190° sector starting from the subsolar point at launch. In these analytic fits the independent variable was the magnetic L parameter. This was done with the hope of studying electron distribution along field lines and to investigate what coupling between the magnetic field and the thermal electrons might become evident.

If we compare the values of the descriptive parameters m and n obtained for the range of sun-earth-satellite angle from 55° to 193°, we see a remarkable similarity, which is not necessarily significant in itself but that points to the fact that on certain days the profiles obtained on the dayside can resemble those obtained on the nightside of earth. As can be seen, all these profiles are approximately uniform in temperature rise and density falloff, yet no two are identical. Individual transits through the magnetosphere show a factor-of-3 variation in density over distances along the orbit of the order of 5000 km. *Cole* [1964] attributes a changing structure in the magnetosphere plasma to random electrostatic fields that cause irreversible energization and transport of ambient plasma from outer to inner parts of the magnetosphere.

The observed electron densities at distances of L equal to 3, 5, and 10, for the time from launch through December 5, 1964, are shown in Figure 6.

These plots represent the observed density over a 2-month period on the dayside of the earth. The angle between the sun-earth-payload line and the precessing orbit line of apsides is shown at the top of the figure (LSEP).

It is apparent from the figure that the observed density is quite variable when viewed on a 2-month time scale. The fluctuations of the $L = 3$ curve and the $L = 5$ curve are larger than the fluctuations at $L = 10$. In addition, a

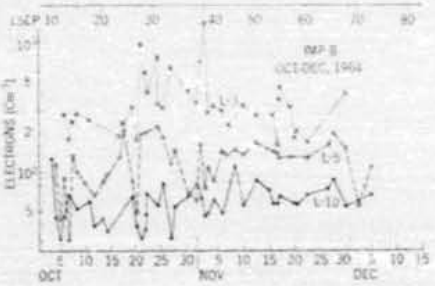

Fig. 6. A summary of observed density variations on different L shells as a function of time in orbit.

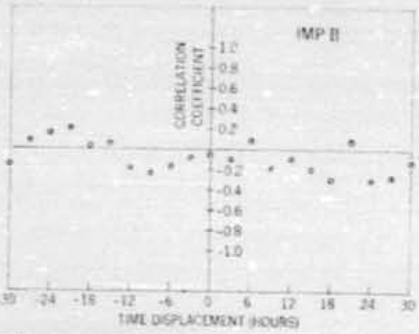

Fig. 7. The cross correlation coefficient between electron density at $L = 3$ and K_p on nonstorm days from October 4 to December 5, 1964, plotted as a function of time displacement between the measurements.

correlation is evident between the large fluctuations at $L = 3$ and at $L = 5$, whereas neither one of these two curves correlates well with the $L = 10$ curve. The observed fluctuations are deemed to be temporal in nature; no systematic variations are noted as the orbit precessed 70° toward the sunrise terminator.

In an attempt to search for a relationship between the geomagnetic field fluctuation and the magnetospheric plasma, we have computed the correlation coefficient between the 3-hour average K_p indices [*Lincoln*, 1965] and the observed electron densities for spacecraft positions on several selected magnetic L shells. The data have been grouped in two classes: (1) data obtained on days having a magnetic disturbance classified as 'moderately severe' and (2) data obtained on other days. For this analysis we have used electron densities obtained during the period October 4 to December 5 on L shells 3, 5, and 10.

To test the effective propagation time relationship between the field fluctuation at the earth's surface and the plasma density at the spacecraft position, the cross correlation coefficient was computed between the magnetic indices K_p (T_o) and the density $n(L,T_o+T)$ for time displacements T in the time interval -30 to $+30$ hours.

Figure 7 shows that for the nonstorm days there is no significant correlation between n and K_p for the time shifts we have considered. We therefore conclude that for the time period of the geomagnetic data that has been used (three-hour averages) there is no generally prevalent stable relationship between the K_p index and the magnetospheric thermal electrons.

For the storm days in the time interval considered, the picture is quite different. Figure 8 shows the cross correlation coefficient as a function of time displacement. Most apparent is the significant correlation evident for the ±6-hour interval about zero time shift. The magnetic control of the plasma indicated by this correlation is interpreted at this time to reflect the mean duration of the storm rather than the details of the magnetic control. Detailed discussion of the time structure and significance of this preliminary storm correlation will be deferred until more data becomes available.

2. *Magnetosheath and solar wind regions.* It has been consistently observed that at some point beyond 5 R_E there is a variable, rapid increase in the energetic component of plasma. A typical example of this is shown in Figure 9 where we have plotted the flux of the energetic residual negative component versus geocentric distance in earth radii. This increase is of the order of a factor of 10 over the energetic component present within the magnetosphere, and its presence constitutes our definition of the magnetosheath boundaries. At the time of this enhancement, there is no significant change in the ambient thermal plasma. The IMP 2 orbit did not penetrate much beyond the shock front,

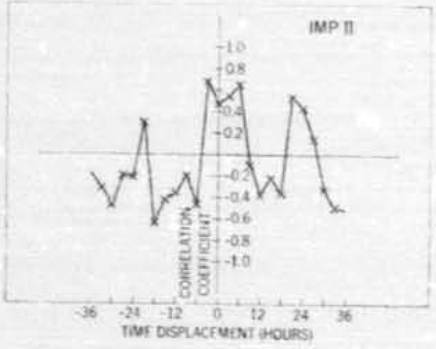

Fig. 8. The cross correlation coefficient between electron density at $L = 3$ and K_p on storm days from October 4 to December 5, 1964, plotted as a function of time displacement between the measurements.

and more detailed discussion of the solar wind region and boundary phenomena is deferred to a later paper in which IMP-C results out to 40 R_E can be included.

Figure 10 is a plot of the observed density at apogee (15.9 R_E) for the period from October 7 to December 5, 1964. Indicated on the figure is the period of time during which apogee occurred in the solar wind region as indicated from our data. For about 10 days after October 25 the shock front was close to spacecraft apogee, and occasional penetration was noted.

From Figure 3 we see that for each orbit the satellite spends more than 10 hours at distances beyond 15 R_E; thus for the period from launch through October 25 we have accumulated a minimum of 120 hours of data in the solar wind region. During this entire period of observation, the average electron density was 50 cm^{-3}. The value of 50 electrons cm^{-3} refers to the density of thermal electrons whose measured temperature lies between 1 and 2 ev.

There have been several measurements of the flux and density of the solar wind. Using a differential energy spectrometer whose lowest energy channel was 230 ev, *Snyder and Neugebauer* [1964] have observed the solar wind velocity to be in the range from 360 to 700 km/sec. Of their observed proton density values 90% were between 0.3 and 10 cm^{-3}. *Bridge et al.* [1965] have used a Faraday cup analyzer whose lowest detectable ion energy was 45 ev (65 ev for electrons) to observe a proton flux of 10^7 to 10^8 cm^{-2} sec^{-1}. Their observed-particle velocity was 250 to 440 km/sec. *Wolfe et al.* [1965] report that the solar wind proton density of particles having a velocity of the order of 560 km/sec rarely exceeds 3 cm^{-3}. Their

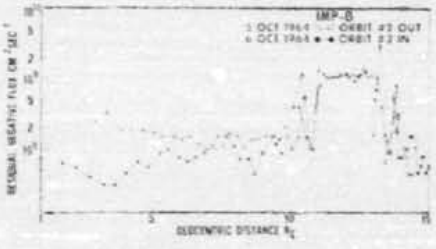

Fig. 9. Plot of the residual negative current flux, observed during the second orbit, as a function of geocentric distance.

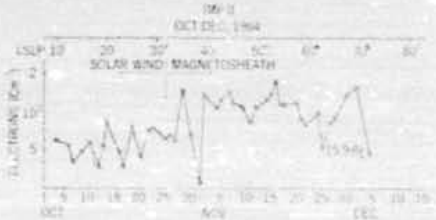

Fig. 10. A summary of observed density variations at apogee (15.9 R_E geocentric) as a function of time in orbit.

minimum detectable energy was 25 ev. Thus there have been no experiments previously reported capable of detecting the presence of low-energy (below 25 ev) protons or electrons.

Present solar wind theory [*Parker*, 1958; 1965] predicts number densities and streaming velocities in agreement with the above cited results for the proton flux. The present theory describes the magnetic field as carried along by the streaming protons. The possibility of a local static plasma is thus excluded by the theory. The present work is the only direct plasma probe measurement of low-energy (below 4 ev) electrons and positive particles in the solar wind region. Our observation of an omnidirectional neutral plasma of density 10 times that of the solar wind is in disagreement with presently accepted solar wind theory.

Electron density measurements in this region have also been obtained from lunar radar reflection observations. *Howard et al.* [1965] interpreted the Doppler shift measurements at two different frequencies in terms of the total columnar electron content between the earth and the moon. They used simultaneous Faraday rotation and ionospheric sounding measurements to correct their measurement for the ionospheric electron content. Assuming a uniform density in cislunar space, they then obtain $30(+70 -150)$ and $100(+70-150)$ cm^{-3} as the average electron densities 35° and 45° from the noon meridian in good agreement with the present results.

To verify the existence of charge neutrality and to exclude the possibility of a significant number of photoelectrons within the spacecraft sheath, we have examined typical ion retardation curves. Figure 11 represents a group of data obtained at 14.0 R_E. At this distance the

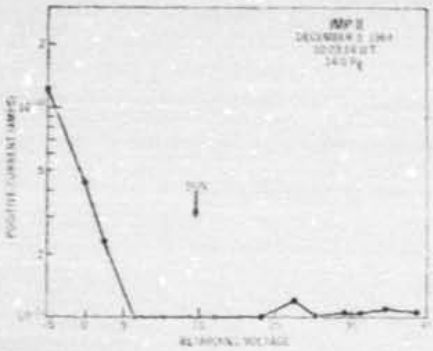

Fig. 11. Sample ion current–voltage retardation curve, the logarithmic positive current is plotted as a function of the linear retardation potential in volts. The five data points symmetric about the sun arrow (crosses) indicate that the electrometer is being driven below zero volts by a negative current component due to photoemission currents from the suppressor grid.

current to the ion trap is governed solely by diffusion since the satellite velocity is approximately 10^5 cm/sec, whereas the velocity of a 2 ev proton is approximately 2×10^7 cm/sec. The presence of ion current retardation near zero volts is not inconsistent with a one-to-two-volt positive satellite potential. Furthermore, it verifies that the potential of the spacecraft is not highly negative. From these data we compute, using the geometric area of the aperture A_a, an ion density of 300 ± 50 protons cm^{-3} at a temperature of 2 ev. The electron density measured at this distance is 350 ± 40 cm^{-3}. From these measurements of aperture currents we conclude that an upper limit for the sum of local photoelectron density and local deviation from strict charge neutrality is (50 ± 65) cm^{-3}.

To put these measurements in their proper perspective, we can investigate the energy content of the various components present in the region beyond the shock front. The results of Bridge, Neugebauer, and Wolfe previously cited all yield an energy density of the order of 2×10^{-9} erg cm^{-3} for the wind component.

The energy density of a 2-ev plasma of density 50 electron-ion pairs per cm^{-3} is 3×10^{-10} erg/cm^{-3}, which is the magnetic energy density

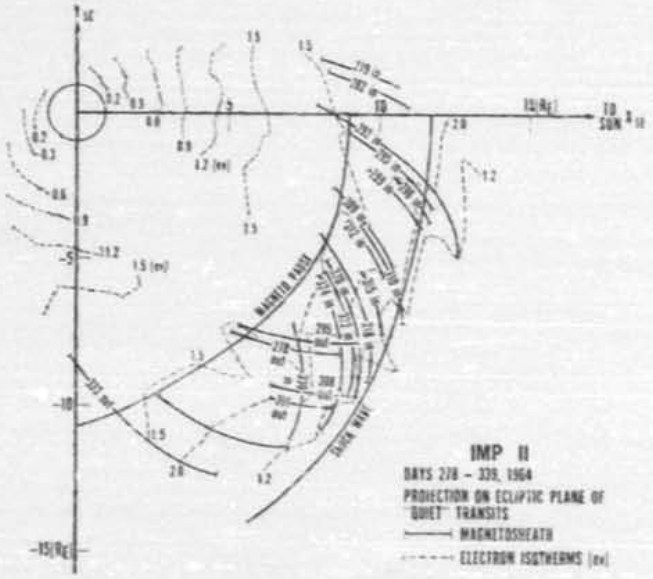

Fig. 12. Projection on ecliptic plane of quiet transits, electron temperature data, and enhanced levels of high-energy electron current component, as a function of days in orbit.

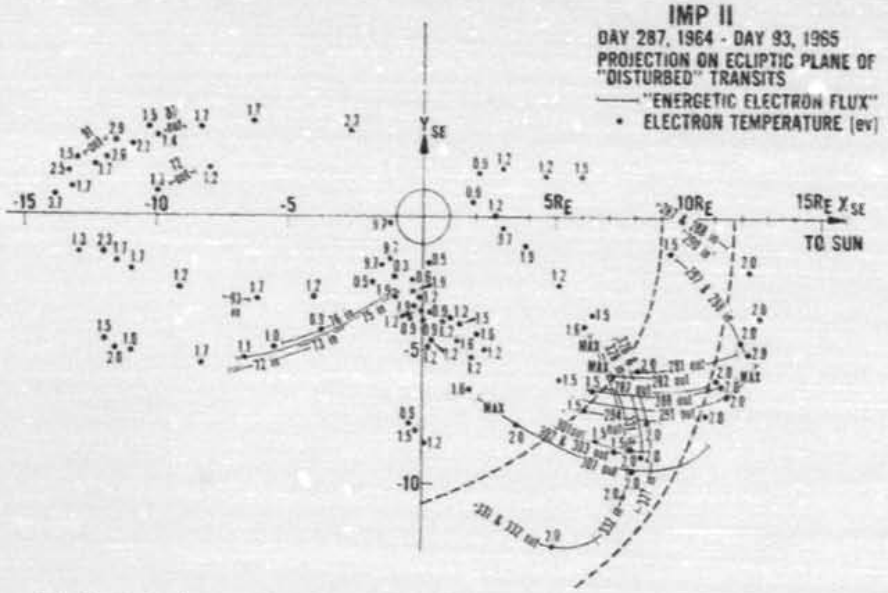

Fig. 13. Projection on ecliptic plane of disturbed transits, electron temperature data, and enhanced levels of high-energy electron current component, as a function of days in orbit.

of a 9-gamma field. Thus the energy density of the thermal plasma and magnetic field is about 1% of the total energy density in the medium.

3. *Summary of results.* Figure 12 is a summary of our observations of thermal electrons in the dayside magnetosphere during selected quiet transits. Shown is a projection onto the ecliptic plane of those traverses during which we observed a uniform increase in temperature with distance and at the same time observed that the ratio of 'thermal' to 'energetic' current components was at least 10 to 1 within the magnetosphere. The shapes of the indicated shock and magnetopause were taken from *Ness et al.* [1964]. Magnetosheath data, indicated by the solid lines in the figure for each day of transit, are characterized by having the ratio of the two currents change abruptly from 10 to 1 to a ratio of 5 to 1 or less. The shock front was then located as a best fit to the data.

The dashed curves in the figure indicate isotherms that can be drawn through the data points, open circles, for each quiet transit. Beyond 5 R_E the thermal electron temperature remains essentially constant even as we cross the magnetopause. The largest temperature value occurs at the inside of the indicated shock front. Beyond the shock front the temperature drops to 1.2 ev. Thermal electrons do not appear to undergo any marked changes in temperature or density across the magnetopause. This generalized picture is supported by all the data presented in Table 1 as well as the plots of Figures 12 and 13. In Figure 13 we have plotted the data characterized as disturbed; as can be seen, isotherms cannot be drawn through the indicated temperature values. Electron temperatures are generally in the range from 1 to 2 ev; the difference between the two conditions is that quiet transits have a more ordered temperature structure. In Figure 13 we observe what seems to be a maximum temperature of 2 ev, which occurs with some consistency near the indicated shock front. On the dark side of the earth, the temperature ranges primarily between 1.2 ev and 2.5 ev; only isolated instances of temperatures lower than 1.0 ev or higher than 2.5 ev have been observed. The appearance of regions of enhanced high-energy electron current components does not correlate with the thermal

or low-energy temperature values. The appearance of the high-energy component current is reminiscent of *Anderson's* [1965] observation of enhanced islands of 40-kev electrons as seen on the dark side with IMP 1.

5. Conclusions

The integral spectrum for low-energy electrons has been measured with detailed definition of temperature and number density throughout the IMP 2 orbit. Electrons are found to have a Maxwellian distribution at energies below 2.0 ev. The electron temperature is found to increase by about a factor of 10 within the distance from 2 to 5 R_E; the increase is generally as the square of the radial distance. In this same region the electron density decreases as the inverse cube of the distance; thus the pressure of the thermal electron gas is falling off approximately inversely proportional to the distance. From 5 R_E to 16 R_E this pressure remains constant. A preliminary check of ion current measurements indicates that ion densities and temperature are in agreement with the electron measurements reported on here. During magnetically disturbed days a statistically significant correlation is found to exist between the measured electron density variation at L shells below 5, and the K_p magnetic index. On all other days the correlation is not statistically significant.

The location of the magnetopause is not evident in the low-energy electrons; the thermal electron density and the temperature remain constant across the magnetopause. An intensity increase is noted in the energetic electron component in the magnetosheath; the boundaries of the magnetosheath can be determined with some consistency on this basis. The density of thermal electrons, 50 cm^{-3}, has been measured at 15.9 R_E, which is presumably in the solar wind region.

References

Anderson, K. A., Energetic electron fluxes in the tail of the geomagnetic field, *J. Geophys. Res., 70*, 4741–4763, 1965.

Angerami, J. J., and D. L. Carpenter, Whistler studies of the plasmapause in the magnetosphere, 2, Electron density and total tube electron content near the knee in magnetospheric ionization, *J. Geophys. Res., 71*, 711–725, 1966.

Bridge, H., A. Egidi, A. Lazarus, E. Lyon, and L. Jacobson, Preliminary results of plasma measurements on IMP-A, *Space Sci., 5*, 969–978, 1965.

Carpenter, D. L., Whistler evidence of a 'knee' in the magnetospheric ionization density profile, *J. Geophys. Res., 68*, 1675–1682, 1963.

Carpenter, D. L., Whistler studies of the plasmapause in the magnetosphere, 1, Temporal variations in the position of the knee and some evidence on plasma motions near the knee, *J. Geophys. Res., 71*, 693–709, 1966.

Carpenter, D. L., and R. L. Smith, Whistler measurements of electron density in the magnetosphere, *Rev. Geophys., 2*, 415–441, 1964.

Cole, K. D., On the depletion of ionization in the outer magnetosphere during magnetic disturbances, *J. Geophys. Res., 69*, 3595–3601, 1964.

Howard, H. T., V. R. Eshleman, G. H. Barry, and R. B. Fenwich, Radar measurements of the total cislunar electron content, *J. Geophys. Res., 70*, 4357–4363, 1965.

Lincoln, J. Virginia, Geomagnetic and solar data, *J. Geophys. Res., 70*, 1229, 1751, and 2231, 1965.

Ness, N. F., C. S. Scearce, and J. B. Seek, Initial results of the IMP 1 magnetic field experiment, *J. Geophys. Res., 69*, 3531–3569, 1964.

Neugebauer, M., and C. W. Snyder, The mission of Mariner 2, preliminary observations, *Science, 138*, 1095–1099, 1962.

Obayashi, T., Ionospheric experiment using the orbiting geophysical observatory (OGO-A) at the Ionosphere Research Laboratory, Kyoto University, *Rept. Ionosphere Space Res. Japan, 19*, 214–224, 1965.

Parker, E. N., Dynamics of the interplanetary gas and magnetic fields, *Astrophys. J., 128*, 664–676, 1958.

Parker, E. N., Dynamical properties of stellar coronas and stellar winds, 5, Stability and wave propagation, *Astrophys. J., 143*, 32–37, 1966.

Parker, L. W., A computer program for calculating the charge distribution about a space vehicle, paper presented at American Astronautical Society, 2nd Symposium on Interaction of Space Vehicles with an Ionized Atmosphere, Miami Beach, Florida, November 1965.

Serbu, G. P., Results from the IMP 1 retarding potential analyzer, *Space Sci., 5*, 564–574, 1965.

Slish, V. I., The measurement of cosmic radio emission at the frequencies 210 and 2200 kc/s at distances up to 5 earth radii, from the Automatic Interplanetary Station Zond 2, *Cosmic Res., Tome III*, 760–767, 1965.

Snyder, C. W., and M. Neugebauer, M., Interplanetary solar wind measurements by Mariner 2, *Space Res., 4*, 89–113, 1964.

Taylor, H. A., Jr., H. C. Brinton, and C. R. Smith, Positive ion composition in the magnetoionosphere obtained from the OGO-A satellite, *J. Geophys. Res., 70*, 5769–5781, 1965.

Wolfe, J. H., R. W. Silva, M. A. Myers, Observations of the solar wind during the flight of IMP 1, *J. Geophys. Res., 71*, 1319–1340, 1966.

(Manuscript received January 27, 1966;
revised April 11, 1966.)

TAC D-01563

EXPLORER XXI

IMP-B, ELECTRON ANALYSIS MERGE OUTPUT TAPE

FORMAT

The IMP-B. Electron analysis merge output tape is a 7 track even parity IBM compatible BCD tape where logical records are 155 bytes (characters) long. The word location assignments and formats are as follows: Blocksize is 2790 bytes, and density is 800 bp:

Character Numbers	Format	Description
1-2	A2	number of points used in fit
3-4	A2	type of fit-1H, 2L, 3H
5	I1	class of fit-1,2,3,channel at which fit start
6-15	E10.2	Ih intercept current at Up of high fit
16-25	E10.2	h slope of high energy fit
26-35	E10.2	I1 intercept current at Vp of fit
36-45	E10.2	1 slope of low energy fit
46-55	E10.2	V_p spacecraft potential
56-65	E10.2	I_2 current at 0-3 retarding volts
66-75	E10.2	N electron density
76-85	E10.2	I_t terminal (high voltage) current
86-95	E10.2	sd (standard deviation) of fit
96-105	E10.2	Lsep approx. sun-earth-probe angle
106-112	I7	Sequence number
113-116	I4	day of year (Julian)*
117-119	I3	hour of day
120-122	I3	minute of day
123-132	E10.2	A mag field in gamma units
133-142	E10.2	B mag L shell in earth radii
143-147	F5.1	distance from center of earth
148-151	I4	longitude
152-155	I4	latitude

*data from 1965 is actual day of year
data from 1966 is actual day of year + 1000 for IMP C
data from 1967 is actual day of year + 2000

data from 1964 is actual day of year for IMP B no overlap of Jul day
data from 1965 is actual day of year

M 48 KODAK

X-615-66-328

THERMAL PLASMA MEASUREMENTS WITHIN THE MAGNETOSPHERE

By

G. P. Serbu
E. J. R. Maier

July 1966

GODDARD SPACE FLIGHT CENTER
Greenbelt, Maryland

THERMAL PLASMA MEASUREMENTS WITHIN THE MAGNETOSPHERE

G. P. Serbu
E. J. R. Maier
Laboratory for Space Sciences
NASA-Goddard Space Flight Center
Greenbelt, Maryland

ABSTRACT

It has been observed that both the ion and electron components of the plasma present within the magnetosphere exhibit, at most times, a Maxwell-Boltzmann energy distribution. The temperature of the electron gas increases by a factor of about 10 from above the ionosphere to an altitude of 2.5×10^4 km ($5R_E$ geocentric). Over this same region, the density decreases to a minimum of about 50 cm^{-3}. Less pronounced variations of temperature and density with radial distance are noted beyond $5R_E$.

The simultaneous observation of ion and electron density profiles provides verification of charge neutrality over vertical dimensions of the order of kilometers.

THERMAL PLASMA MEASUREMENTS WITHIN THE MAGNETOSPHERE

G. P. Serbu and E. J. R. Maier

INTRODUCTION

The satellite IMP-II was launched on 4 October, 1964, into an elliptical orbit with a period of 36 hours. The initial perigee was 200 km and the apogee was 95,000 km (15.9R_E geocentric).

Figure 1 is a polar plot of the IMP-II orbit as seen in geographic latitude and earth radii (R_E) coordinates. At launch the apogee was 20° below the ecliptic plane, with the sun-earth payload angle (LSEP) of 11°. This orbit has offered a good opportunity to investigate the magnetosphere on the dayside of earth near the equatorial plane.

On-board IMP-II was a retarding potential analyzer, which measured the integral spectrum of ions and electrons in the energy interval from 0 to 45 eV. The details of this experiment have been discussed elsewhere, [1]. Briefly stated, the experiment consists of performing a measurement of the collector current as a function of retarding potentials. The retarding potentials used in the measurement are programmed as indicated in Figure 2. The voltage program defines the electron, ion, and net current modes. The electrometer polarity is programmed to give an analog output from 0 to 5 volts for negative currents during the electron mode. The electrometer polarity is then reversed in order to measure only positive currents during the ion mode. The effective aperture area of the Faraday cup sensor is 5 cm^2. Particles within an acceptance cone of 170° are accelerated through the aperture and subsequently collected. Photoemission currents from the collector have been successfully suppressed during the electron mode and the 45 volt ion mode. Photoemission currents from the suppressor grid can, however, reach the collector and must be accounted for in the analysis.

RESULTS

In Figure 3 are plotted two retardation curves obtained on 27 March 1965 while IMP-II was in the nightside magnetosphere on an inbound orbit at a distance between 3.9 and 3.4R_E. Shown on the left is the negative current response plotted on a log scale as a function of the retarding potential in volts in the interval from +5 to -45 volts. The dots and crosses represent two individual curves which were obtained

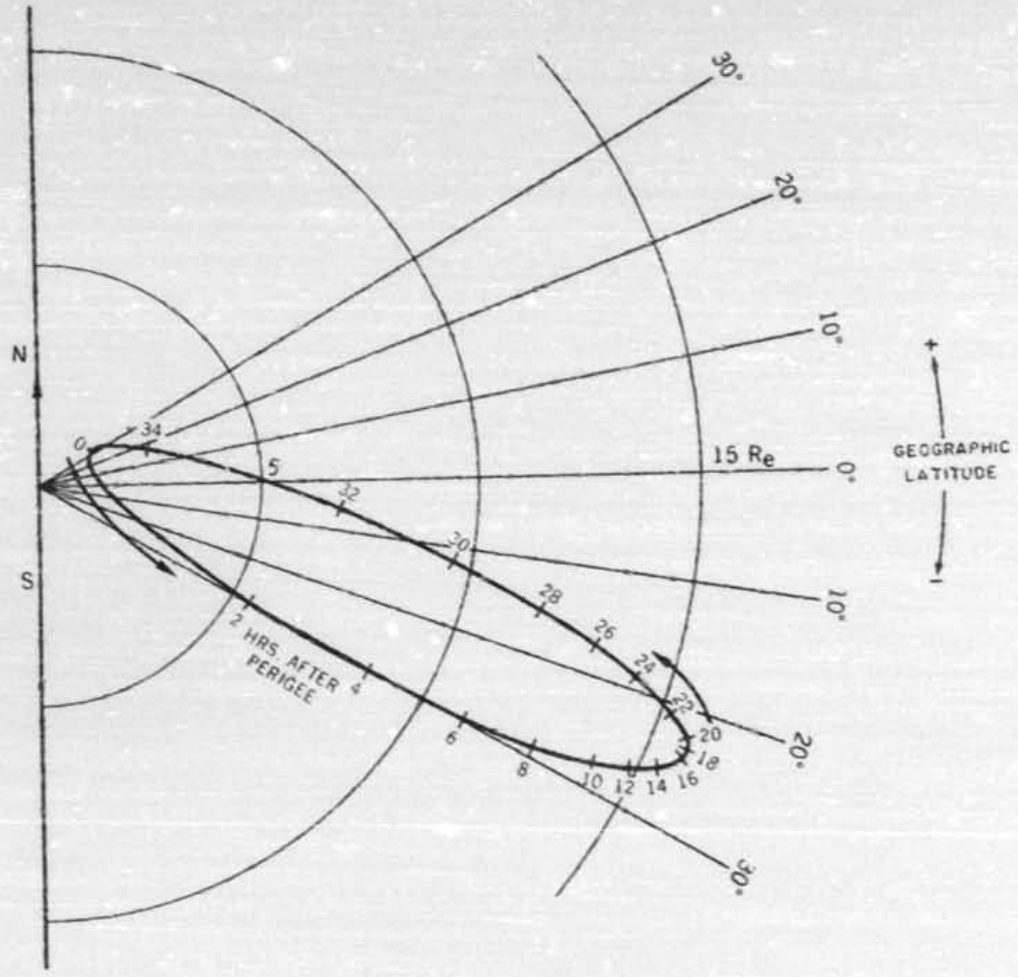

Figure 1. A view of the latitudinal excursion of the IMP-II spacecraft. IMP-II was launched with the line of apsides extending toward the sun, but inclined about -20° to the ecliptic.

sequentially within 11 minutes of each other, during this time interval the satellite traversed $0.3R_E$. The arrow in the figure at -35 volts indicates that at this time the plane containing the sun-payload vector was normal to the sensor. The measurements made to within ±85° of the sun contain photoemission currents from the suppressor grid and a correction for this current component should be made on the five data points, symmetric about the sun vector arrow.

IMP-B
RETARDING POTENTIAL ANALYSER

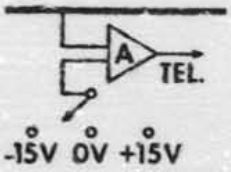

	ELECTRON		ION		NET CURRENT	
APERTURE	+50	+15	-50	-15	0	0
RETARDING	-45→0	-15→0	0→+45	0→+15	0	0
SUPPRESSOR	0	0	-50	-15	0	0
COLLECTOR	+15	+15	-15	-15	0	0
ELECTROMETER POLARITY	-	-	+	+	-	+

Figure 2. Schematic representation of the sensor and the experiment voltage program.

The wave form of the current response as a function of retarding potential in the interval from +5 to -10 volts can be analyzed in accordance with the Langmuir probe theory for the collection of diffusive currents, which are due to a plasma component having a Maxwell-Boltzmann distribution of velocities. Using this analysis procedure, the electron temperature as measured from the slope of the curve is 3.2 ± 0.2 eV at $3.9R_E$ and 2.5 ± 0.2 eV at $3.6R_E$.

We have observed, in the dayside magnetosphere, on selected days [1] that a well ordered electron temperature structure is present independent of the LSEP angle. For example, in the region from 2 to $5R_E$ the electron temperature increases from 0.3 eV at $2R_E$ to 1.6 eV at $5R_E$. The temperature increase over this region as a function of radial distance can be expressed as $T_e \propto R_e^{+1.9}$. A less pronounced temperature increase is noted at distances beyond $5R_E$.

The data for 27 March 1965 was obtained in the nightside magnetosphere, LSEP ~ 190°. These nightside electron temperature values are about a factor of 3 higher than the corresponding values taken from the dayside temperature profile. Whether spatial or temporal variations are involved cannot be resolved on the basis of these isolated temperature measurements. The 27 March 1965 data, Figures 3 and 4, have been selected to illustrate in detail how electron and ion curves are analyzed; we will be discussing additional data obtained in the dayside magnetosphere.

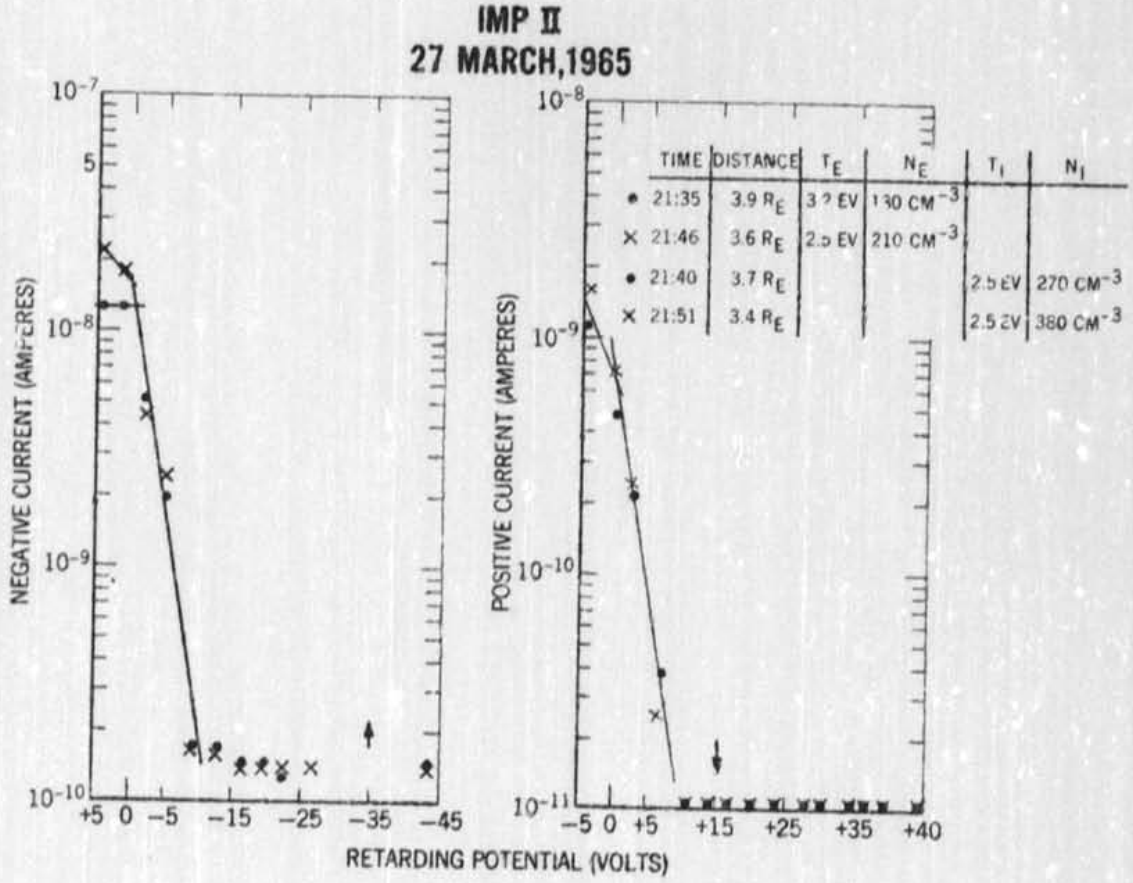

Figure 3. Sample plots of negative and positive current response as a function of retardation voltage. This data was obtained while IMP-II was on an inbound orbit in the nightside magnetosphere.

From the inflection near zero volts of the electron retardation curve in Figure 3 we measure the satellite to plasma potential to be 0 ± 0.5 volts. At attractive potentials, i.e., to the left of 0 volts, the curve exhibits electron current saturation. Using the measured electron temperature in conjunction with the value of the current at the satellite potential we obtain an electron density of 130 electrons cm^{-3} at $3.9R_E$ and 210 cm^{-3} at $3.6R_E$.

The right hand side of Figure 3 shows the measured positive current plotted on a log scale as a function of the retardation voltage. The wave form of the ion current also exhibits a Maxwell-Boltzmann distribution and so Langmuir probe analysis can be used to determine the ion temperature and density. Since the positive current is retarded almost two orders of magnitude as the retarding voltage is changed from -5 to +7 volts, we can measure the slope of the line as drawn through these data points in order to obtain the ion temperature. From this measurement we obtain a value of 2.5 ± 0.5 eV. Assuming that the predominant ion at this altitude ($3.9R_E$) is H^+, we compute the most probable ion velocity to be about 30 km/sec. for a 2.5 eV temperature, at $4R_E$ where the satellite velocity is 4 km/sec. Since at this altitude the ion velocity is much larger than the satellite velocity, no corrections for the sensor orientation with respect to the velocity vector [2] need to be made.

It is evident in the figure that an inflection in the ion curves occurs at about zero volts, the -5 volts data point is thus in the ion current saturation region. It is not readily evident when examining the curves at precisely what voltage current saturation occurs; obviously, there is an inflection between -5 and 0 volts but the shape of the curve in this interval is not known. Since the saturation point occurs at the satellite potential, its value can be determined with accuracy from the negative current measurement and used to obtain the value of the ion current at saturation. Knowing the value of the ion current at saturation, and the measured ion temperature, we compute ion densities of 270 cm^{-3} at $3.7R_E$ and 380 cm^{-3} at $3.4R_E$.

In computing densities we assign an augmentation factor of 4 to the entrance aperture; this is due to the attractive potential of the aperture. For a more detailed discussion of the augmentation factor, the interested reader is referred to our previous paper [1].

In the legend of Figure 3, we have tabulated the electron and ion densities (N_e, N_i) and the electron and ion temperatures (T_e, T_i). Good agreement is noted between the measured electron and ion

temperatures. The ion density is, within a factor of two, in agreement with the electron density. The factor of two discrepancy is due in part to the previously discussed errors associated with the exact value of the ion current at saturation. Thus, within the limits of the measurement we have determined that the plasma is neutral, at a temperature of about 3.0 eV, and that the spacecraft potential with respect to the plasma is near zero volts.

On this same inbound orbit of 27 March 1965, we have obtained a series of measurements which illustrate how a detailed density profile can be obtained. In Figure 4, we plot five separate ion retardation curves. For reasons of space, we do not show the data beyond +7 volts of retardation since they are all similar to the previously shown curves. In the legend, we note that from 21:35 UT. to 22:24 UT. the satellite was inbound from 3.9 to $1.9R_E$; the trajectory was near the magnetic equator and northbound. From the electron curves, not shown here, we have determined that for this time interval the satellite potential is 0.5 ± 0.25 volts. The previously discussed analysis procedure has been used for each of the curves to obtain a detailed density profile in the nightside magnetosphere region from 3.7 to $1.9R_E$. Note that for the curve marked $2.3R_E$ the data point at -5 volts is a factor of ten lower than expected, thus no specific value of density at this radial distance can be obtained; however, the remaining portion of that curve is in general agreement with the preceding and subsequent curves.

The results of our density measurements are plotted in the lower right hand corner of Figure 4 on a log scale as a function of the radial distance. Included in the plot of density vs. R_E are values of electron density (asterisk symbol) and values of ion density. The error bar for the ion density is taken to be a factor of 2, whereas the electron density error bar is less than 15%. It is seen that within the limits of the error bar, the values of ion and electron densities are equal, and thus the measurement indicates a neutral plasma with a density of the order of 10^3 cm^{-3} at 2 R_E which falls off according to a power law of the radial distance.

In Figure 5, we plot the measured density and temperature profiles for both ions and electrons, obtained with the dayside magnetosphere for the two successive inbound orbits of 28 and 30 October 1964. These two orbits occurred at a sun-earth-payload angle (LSEP) of 38°, thus they are representative of the dayside magnetosphere. Log-log scales have been used to plot the particle density cm^{-3}, and temperature (eV) as a function of geocentric distance R_E. In the figure the crosses

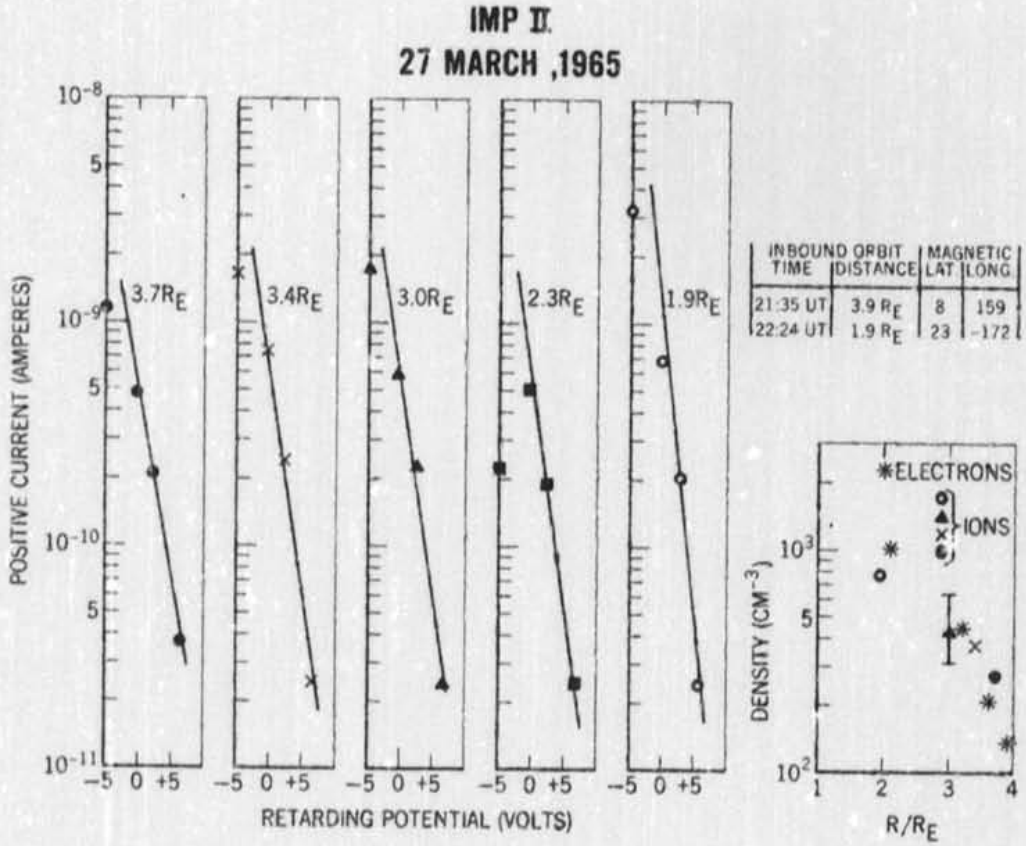

Figure 4. Five consecutive ion retardation curves are plotted for the inbound orbit of 27 March 1965. The ion density computed from these curves is plotted along with the electron density as a function of geocentric distance.

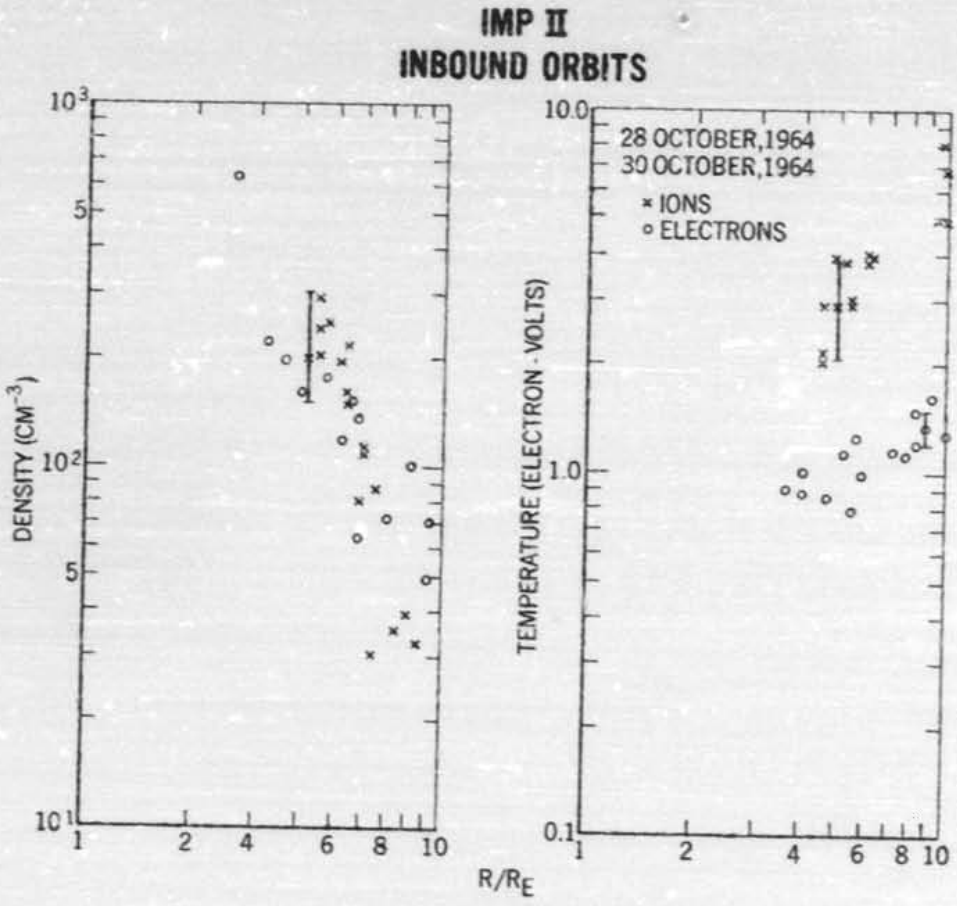

Figure 5. Electron and ion density and temperature are plotted as a function of geocentric distance. These data were obtained while IMP-II was near the ecliptic plane in the dayside magnetosphere.

represent the ion data and the open circles are for the electron data. The average fall-off rate of the density profile may be approximated by a R_E^{-4} relationship. Spatial deviations from a smooth fall-off rate are noted; however, there is no evidence for a large drop of "KNEE" in the density profile, as has been reported by Carpenter [3].

Slish [4] has recently reported the results of an antenna impedance measurement associated with cosmic noise observations by an experiment on the spacecraft Zond II, launched November 1964. Two independent observations are presented. A peak attributed to electron plasma resonance was observed in the 210 kc/s receiver response at $4R_E$ geocentric. This observation yields a local density of 550 electrons cm^{-3}. The second observation is an analysis of the receiver response to a signal above the plasma frequency in terms of the effect of the local plasma density on the radiation resistance of the antenna. Interpreted in this manner, a radial dependence $N_e = 1.3 \times 10^5 (R/R_0)^{-4}$ valid from 4 to $7R_E$ is obtained. Both the general radial dependence and the specific value of 100 electrons cm^{-3} at $6R_E$ are in agreement with our results.

Obayashi [5] has used the differential Doppler shift of the harmonically related transmitters (40 and 360 Mc/s) on OGO-A to determine the local electron density in the vicinity of the spacecraft. He obtains an average local density at local noon on 16 November 1964, of 1 to 2×10^3 cm^{-3} at a geocentric distance of $3.2R_E$. The IMP-II satellite was at $3.3R_E$ on 16 November 1964 at 11:03 UT.; the density value as measured by us was 1.04×10^3 electrons cm^{-3}.

In Figure 5, the temperature profiles for ions and electrons as a function of geocentric distance are in general agreement in the rate of temperature increase with distance; however, we note that the ion temperature is higher than the electron temperature, taking into account the appropriate errors. It appears that near the magnetopause, approximately $10R_E$, the ratio of ion-to-electron temperature is higher than that at $5R_E$. We suggest that this preliminary observation might possibly be interpreted as follows: In the magnetosheath, solar wind energy is transferred to the thermal ions raising their temperature well above that of the thermal electrons. The electron temperatures in the magnetosheath have been observed to be between 1 and 3 eV [1]. Theoretical treatments of the detailed process involved in thermalization of the solar wind have been presented by Scarf, et.al. [6] who suggested that solar wind ions lose speed in the sub-solar magnetosheath resulting in the generation of ion-waves and that the electric fields

associated with the waves allow fast diffusion of plasma into the magnetosphere. Eviatar [7] finds that the interaction with electron plasma oscillations are effective in scattering super-thermal electrons and that ion waves are the dominant mechanism for the diffusion of sub-thermal (1 eV) electrons across the magnetopause.

It appears that within the magnetosphere, the ion temperature decreases from its relative high value in the magnetosheath, due to heat transfer to the electrons. Such a mechanism could explain the thermal gradients in the magnetosphere, and account for the fact that the ion-to-electron temperature ratio decreases with distance from the magnetopause.

CONCLUSIONS

The results of successive and continuous measurements of positive and negative retardation currents within the magnetosphere have been presented. Our interpretation of these measurements are summarized as follows:

1. Electrons and ions have a Maxwell-Boltzmann distribution of velocities in the thermal energy range of the order of eV; these particles constitute a neutral plasma.

2. Within $5R_E$ in the magnetosphere we observe a temperature profile which increases approximately as the square of the radial distance, while the density profile exhibits a decay that can be approximated by the inverse third to fourth power of the radial distance.

3. Our measurements of particle density do not indicate a whistler "KNEE" phenomenon. In fact, we observe 10 to 50 times as large a density beyond the "KNEE" as has been reported from whistler results.

REFERENCES

1. G. P. Serbu, E. J. R. Maier, to be published in J. Geophys. Res. 71 (1966), No. 15.

2. E. C. Whipple, Goddard Space Flight Center Report X-615-65-296, 1965.

3. D. L. Carpenter, J. Geophs. Res., Vol. 71, No. 3.

4. V. I. Slish, Cosmic Research, Tome III.

5. T. Obayashi, Report of Ionosphere and Space Research in Japan, Vol. 19, No. 2.

6. F. L. Scarf, W. Bernstein and R. W. Fredericks, J. Geophys. Res. 70 (1965), No. 1.

7. A. Eviatar, J. Geophys. Res. 71 (1966), No. 11.

DAT 528 = OCT 4 1964

```
123M1  3.59E-10  1.13E 02  1.60E-09  1.35E 00 -1.20E 00  3.34E-09  2.13E 02
0E 01    106 278  5 10  6.00E 02  6.10E 00  4.1  94 -35132M1  3.38E-10  1.5
 -6.51E-02  3.34E-09  1.71E 02  2.63E-10  1.11E-01 -1.20E 01    106 278  5
.1  94 -35141M1  3.36E-10  1.60E 02  3.25E-09  2.17E 00  6.57E-02  3.34E-09
0E-01 -1.20E 01    106 278  5 10  6.00E 02  6.10E 00  4.1  94 -35113L2  3.4
  1.23E 00  2.44E-02  4.61E-09  3.08E 02  3.34E-10  7.08E-02 -1.20E 01    1
.10E 00  4.1  94 -35131L2  3.42E-10  0.0        4.30E-09  1.26E 00  8.80E-02
4E-10  6.39E-02 -1.20E 01    107 278  5 11  6.00E 02  6.10E 00  4.1  94 -35
  1.91E-09  9.20E-01 -1.68E 00  3.34E-09  2.58E 02  3.17E-10  9.75E-02 -1.2
.78E 02  7.29E 00  4.9  95 -35 53M3  4.48E-10  6.92E 03  0.0        0.0
        4.37E-10  5.53E-02 -1.20E 01    138 278  5 53  2.39E 02  8.54E 00  5
  1.64E 02  1.77E-09  1.08E 00 -1.34E 00  3.93E-09  2.80E 02  4.22E-10  5.0
8  6 15  1.76E 02  9.38E 00  6.3  95 -35132M1  4.77E-10  3.82E 02  4.14E-09
4E-09  2.17E 02  4.22E-10  1.66E-01 -1.19E 01    154 278  6 15  1.76E 02  9
  4.74E-10  4.06E 02  3.93E-09  2.05E 00  1.07E-01  4.14E-09  2.14E 02  4.2
    154 278  6 15  1.76E 02  9.38E 00  6.3  95 -35123L2  4.44E-10  0.0
5E-01  5.13E-09  3.68E 02  4.37E-10  4.59E-02 -1.19E 01    155 278  6 16  1
5 -35131L2  4.29E-10  0.0        5.16E-09  1.23E 00 -5.13E-03  5.13E-09  3.4
 -1.19E 01    155 278  6 16  1.76E 02  9.38E 00  6.3  95 -35103M3  4.22E-10
       0.0        0.0        0.0        3.17E-10  9.49E-02 -1.19E 01    202 27
01  8.0  88 -33123M3  3.72E-10  1.25E 02  0.0        0.0        0.0        3.0
  8.76E-02 -1.19E 01    218 278  7 42  6.66E 01  1.19E 01  8.6  84 -32123M1
0E-09  7.98E-01 -1.63E 00  6.55E-09  5.42E 02  6.97E-10  2.03E-01 -1.18E 01
01  1.26E 01  9.4  78 -30142M1  1.03E-09  8.16E 01  5.57E-09  2.95E 00  7.1
  6.97E-10  2.73E-01 -1.18E 01    234 278  8 25  4.90E 01  1.26E 01  9.4  7
5E 01  5.72E-09  2.65E 00  5.70E-01  7.09E-09  3.22E 02  6.97E-10  2.36E-01
26  4.90E 01  1.26E 01  9.4  78 -30123L2  7.47E-10  0.0        2.16E-09  9.1
  5.35E 02  8.21E-10  1.79E-01 -1.18E 01    235 278  8 27  4.73E 01  1.26E

151L2  7.39E-10  0.0        6.31E-09  1.03E 00  9.29E-02  6.91E-09  5.04E 02
8E 01    235 278  8 27  4.73E 01  1.26E 01  9.5  77 -30103M3  8.99E-10  8.9
  0.0        6.62E-09  0.0        8.84E-10  2.28E-01 -1.18E 01    266 278  9
.3  71 -28 73M3  1.39E-09  3.55E 01  0.0        0.0        0.0        0.0
6E-01 -1.18E 01    282 278  9 31  3.27E 01  1.34E 01 10.6  67 -27123L2  1.3
  1.51E 00  2.94E-01  8.77E-09  5.28E 02  1.50E-09  7.49E-02 -1.18E 01    2
.36E 01 11.0  63 -26131L2  1.39E-09  0.0        7.34E-09  1.49E 00  2.64E-01
0E-09  7.11E-02 -1.18E 01    299 278  9 55  2.87E 01  1.36E 01 11.0  63 -26
  3.40E-09  4.65E-01 -1.91E 00  6.40E-09  6.94E 02  1.12E-09  7.99E-02 -1.1
.60E 01  1.38E 01 11.3  59 -25123L2  1.78E-09  0.0        2.87E-09  1.71E 00
3E 02  1.76E-09  3.90E-02 -1.17E 01    315 278 10 16  2.60E 01  1.38E 01 11
  0.0        7.71E-09  1.40E 00  3.29E-01  9.76E-09  6.11E 02  1.76E-09  4.9
8 10 16  2.60E 01  1.38E 01 11.3  59 -25123L2  1.22E-10  0.0        1.53E-09
7E-09  1.98E 02  1.21E-10  1.63E-01 -1.17E 01    403 278 12 17  1.63E 01  1
  1.23E-10  0.0        3.30E-09  1.63E 00  8.36E-02  3.47E-09  2.01E 02  1.2
    403 278 12 17  1.63E 01  1.47E 01 13.0  36 -20123M1  2.95E-10  2.99E 01
6E 00  2.56E-09  1.64E 02  8.70E-11  1.64E-01 -1.17E 01    418 278 12 37  1
2 -19132M1  2.76E-10  3.43E 01  2.67E-09  2.24E 00 -2.18E-01  2.43E-09  1.2
 -1.17E 01    418 278 12 37  1.53E 01  1.49E 01 13.2  32 -19141M1  2.68E-10
9E 00  5.13E-04  2.43E-09  1.16E 02  8.70E-11  1.76E-01 -1.17E 01    418 27
01 13.2  32 -19123L2  2.59E-10  0.0        2.20E-09  1.30E 00  2.13E-02  5.6
  1.05E-01 -1.17E 01    427 278 12 49  1.47E 01  1.50E 01 13.4  30 -19141L2
0E-09  1.31E 00  6.01E-02  5.65E-09  3.65E 02  2.43E-10  1.05E-01 -1.17E 01
01  1.50E 01 13.4  30 -19 93M3  4.64E-10  2.73E 01  0.0        0.0        0.0
  1.52E-10  1.62E-01 -1.16E 01    442 278 13 10  1.39E 01  1.51E 01 13.5  2
0E 02  1.33E-09  1.77E 00 -9.45E-01  2.70E-09  1.50E 02  1.67E-10  1.39E-01
32  1.32E 01  1.52E 01 13.8  22 -17123L2  1.94E-10  0.0        1.27E-09  1.4
  0.0        1.00E 00  4.54E-02 -1.16E 01    459 278 13 33  1.31E 01  1.52E

113M3  2.55E-10  4.63E 01  0.0        0.0        0.0        2.37E-09  0.0
6E 01    474 278 13 53  1.25E 01  1.54E 01 14.0  17 -17113M3  5.55E-10  1.7
  0.0        0.0        0.0        1.01E-10  8.66E-02 -1.16E 01    490 278 14
.2  13 -16 63M3  2.48E-10  1.15E 02  0.0        0.0        0.0        0.0
1E-02 -1.16E 01    506 278 14 37  1.14E 01  1.56E 01 14.4   8 -16123M1  4.0
```

```
1.34E-09  2.13E 02  2.63E-10  2.95E-02 -1.2  REC     1. LENGTH  2790
2H1  3.38E-10  1.56E 02  3.45E-09  2.10E 00
 01     106 278  5 10  6.00E 02  6.10E 00  4
5.57E-02  3.34E-09  1.68E 02  2.63E-10  1.1
  94 -35113L2  3.43E-10  0.0        1.70E-09
-02 -1.20E 01     107 278  5 11  6.00E 02  6
1.26E 00  8.80E-02  4.61E-09  3.04E 02  3.3
5E 00  4.1  94 -35123H1  5.16E-10  6.35E 01
-10  9.75E-02 -1.20E 01     122 278  5 31  3
0.0        0.0        0.0        0.0        0.0
3E 02  8.54E 00  5.7  96 -35123H1  5.31E-10
 02  4.22E-10  5.07E-02 -1.19E 01     154 27
3.82E 02  4.14E-09  1.99E 00  2.48E-03  4.1
 6 15  1.76E 02  9.38E 00  6.3  95 -35141H1
-09  2.14E 02  4.22E-10  1.60E-01 -1.19E 01
4.44E-10  0.0        2.26E-09  1.07E 00 -3.2
  155 278  6 16  1.76E 02  9.38E 00  6.3  9
-03  5.13E-09  3.43E 02  4.37E-10  7.02E-02
-35103H3  4.22E-10  1.18E 02  0.0        0.0
1.19E 01     202 278  7 21  8.33E 01  1.13E
     0.0        3.01E-09  0.0        2.85E-10
  8.6  84 -32123H1  1.38E-09  5.58E 01  3.2
2.03E-01 -1.18E 01     234 278  8 26  4.90E
-09  2.95E 00  7.11E-01  7.09E-09  3.05E 02
  1.26E 01  9.4  78 -30161H1  1.15E-09  8.2
5.97E-10  2.36E-01 -1.18E 01     234 278  8
     2.16E-09  9.16E-01 -1.33E-01  6.91E-09
  4.73E 01  1.26E 01  9.5  77 -30

.91E-09  5.04E 02  8.21E-10  1.67E-01 -1.1  REC     2. LENGTH  2790
H3  8.99E-10  8.93E 02  0.0        0.0
 01     266 278  9 10  3.67E 01  1.32E 01 10
.0         0.0        0.0        6.03E-10  1.7
  67 -27123L2  1.39E-09  0.0        3.26E-09
-02 -1.18E 01     299 278  9 55  2.87E 01  1
.49E 00  2.64E-01  8.77E-09  5.31E 02  1.5
E 01 11.0  63 -26123H1  2.96E-09  3.61E 01
-09  7.99E-02 -1.17E 01     314 278 10 15  2
.87E-09  1.71E 00  8.89E-01  9.76E-09  5.5
E 01  1.38E 01 11.3  59 -25141L2  1.82E-09
02  1.76E-09  4.92E-02 -1.17E 01     315 27
.0         1.53E-09  1.63E 00  1.69E-01  3.4
 17  1.63E 01  1.47E 01 13.0  36 -20151L2
09  2.01E 02  1.21E-10  1.44E-01 -1.17E 01
.95E-10  2.99E 01  1.27E-09  1.33E 00 -1.2
 418 278 12 37  1.53E 01  1.49E 01 13.2  3
01  2.43E-09  1.20E 02  8.70E-11  1.80E-01
19141H1  2.68E-10  3.53E 01  2.43E-09  2.3
.17E 01     418 278 12 37  1.53E 01  1.49E
00  2.13E-02  5.65E-09  3.67E 02  2.43E-10
13.4  30 -19141L2  2.58E-10  0.0        5.4
.05E-01 -1.17E 01     427 278 12 49  1.47E
     0.0        0.0        0.0        0.0
 1.51E 01 13.5  25 -18123H1  2.21E-10  1.2
.67E-10  1.39E-01 -1.16E 01     458 278 13
     1.27E-09  1.26E 00  0.0        0.0
 1.31E 01  1.52E 01 13.8  21 -17

.37E-09  0.0        1.24E-10  1.66E-01 -1.1  REC     3. LENGTH  2790
H3  5.55E-10  1.79E 01  0.0        0.0
 1     490 278 14 15  1.20E 01  1.55E 01 14
.0         0.0        0.0        1.00E 00  9.4
  8 -16123H1  4.00E-10  4.00E 01  2.26E-09
```

64-060A-01A

IDP-2
Explorer 21, Retarding Potential Analyzer

10/4/64 - 4/5/65

Partial dump of D-01563

```
  1.56E 00  0.0        0.0        0.0        1.00E 00  1.73E-01 -1.16E 01     52
.58E 01 14.5    3 -16123H1   4.04E-10   3.94E 01   1.76E-09   1.75E 00   0.0
0E 00  1.37E-01 -1.15E 01     562 278 15 53  1.02E 01  1.61E 01 14.9   -8 -15
  0.0        0.0        0.0        0.0        0.0        1.00E 00  4.15E-03 -1.15
.90E 00  1.62E 01 15.0 -12 -15103H3  2.59E-10  7.86E 01   0.0        0.0
        1.78E-10  5.69E-02 -1.15E 01     594 278 16 37  9.70E 00  1.64E 01 15.
  4.88E 01  1.46E-09  1.72E 00   0.0        0.0        0.0        1.00E 00  4.51
8 17 43  9.20E 00  1.68E 01 15.5 -31 -16113H3  3.05E-10  4.51E 01   0.0
0E-09   0.0        1.42E-10   6.51E-02 -1.14E 01     658 278 18  4  9.10E 00  1.
  2.27E-10  1.06E 02  1.92E-09  1.65E 00 -1.33E 00  3.26E-09  1.87E 02  1.62
    698 278 18 59  9.00E 00  1.73E 01 15.7 -47 -17142H1  1.66E-10  2.71E 03
2E-01  3.51E-09  1.59E 02  1.62E-10  1.84E-01 -1.14E 01     698 278 18 59  9.
7 -17161H1  1.68E-10  1.52E 03  3.22E-09  2.63E 00  2.27E-01  3.51E-09  1.60
 -1.14E 01     698 278 18 59  9.00E 00  1.73E 01 15.7 -47 -17123L2  1.11E-10
4E 00  3.36E-01  5.06E-09  3.02E 02  1.07E-10  1.97E-01 -1.14E 01     699 278
01 15.7 -47 -17141L2  1.15E-10  0.0        4.72E-09  1.43E 00  9.82E-02  5.06
  1.83E-01 -1.14E 01     699 278 19  0  9.00E 00  1.73E 01 15.7 -47 -17 23H3
        0.0        0.0        0.0        0.0        1.00E 00  0.0        -1.14E 01
00  1.74E 01 15.8 -81 -18123H1  2.82E-10  7.22E 01   2.02E-09  1.58E 00 -1.52
  1.67E-10  1.47E-01 -1.14E 01     730 278 19 43  9.00E 00  1.76E 01 15.8 -56
9E 02  3.47E-09  2.65E 00 -3.90E-01  3.00E-09  1.36E 02  1.67E-10  2.13E-01
43  9.00E 00  1.76E 01 15.8 -56 -19123L2  1.71E-10  0.0        2.27E-09  1.31
  2.95E 02  1.60E-10  1.58E-01 -1.14E 01     731 278 19 44  9.00E 00  1.76E 0

131L2  1.66E-10  0.0        4.81E-09  1.41E 00 -7.60E-02  4.56E-09  2.84E 02
4E 01     731 278 19 44  9.00E 00  1.76E 01 15.8 -56 -19103H3  1.97E-10  1.25
  0.0        3.00E-09  0.0        1.50E-10  6.18E-02 -1.13E 01     746 278 20
.9 -61 -19123L2  1.22E-10  0.0        1.92E-09  1.61E 00  2.57E-01  4.74E-09
8E-01 -1.13E 01     747 278 20  6  9.00E 00  1.78E 01 15.9 -61 -19151L2  1.24
  1.53E 00  7.74E-02  4.74E-09  2.84E 02  1.16E-10  2.22E-01 -1.13E 01     74
.78E 01 15.9 -61 -19132H1  2.70E-10  5.75E 01   3.04E-09  2.45E 00   0.0
4E-10  1.79E-01 -1.13E 01     762 278 20 26  9.00E 00  1.79E 01 15.9 -65 -201
  1.86E-09  1.37E 00  2.65E-02  4.56E-09  2.88E 02  1.44E-10  1.43E-01 -1.13
.20E 00  1.82E 01 15.9 -75 -21141L2  1.43E-10  0.0        4.43E-09  1.37E 00
8E 02  1.44E-10  1.30E-01 -1.13E 01     795 278 21 11  9.20E 00  1.82E 01 15.
  5.64E 01  2.02E-09  1.52E 00 -1.51E 00  3.18E-09  1.91E 02  1.39E-10  9.61
8 22  4  9.50E 00  1.87E 01 15.9 -87 -23132H1  2.40E-10  7.57E 01   3.28E-09
2E-09  1.66E 02  1.39E-10  1.81E-01 -1.13E 01     834 278 22  4  9.50E 00  1.
  2.39E-10  7.57E 01   3.28E-09  2.46E 00  1.71E-01  3.52E-09  1.66E 02  1.39
    834 278 22  4  9.50E 00  1.87E 01 15.9 -87 -23123L2  1.54E-10  0.0
5E-01  4.83E-09  3.02E 02  1.47E-10  1.33E-01 -1.13E 01     835 278 22  6  9.
7 -23141L2  1.55E-10  0.0        4.62E-09  1.37E 00  6.20E-02  4.83E-09  3.05
 -1.13E 01     835 278 22  6  9.50E 00  1.87E 01 15.9 -87 -23123H1  3.19E-10
8E 00 -1.27E 00  3.51E-09  2.14E 02  1.90E-10  1.06E-01 -1.12E 01     882 278
01 15.8-102 -26132H1  3.01E-10  8.92E 01   3.60E-09  2.24E 00  5.88E-02  3.70
  1.60E-01 -1.12E 01     882 278 23 10  1.00E 01  1.92E 01 15.8-102 -26141H1
1E-09  2.27E 00  1.18E-01  3.70E-09  1.82E 02  1.90E-10  1.52E-01 -1.12E 01
01  1.92E 01 15.8-102 -26113H1  3.29E-10  6.80E 01   1.86E-09  1.46E 00 -1.27
  1.97E-10  1.91E-01 -1.12E 01     898 278 23 32  1.02E 01  1.94E 01 15.7-106
9E 01  3.51E-09  2.30E 00  1.16E-01  3.70E-09  1.80E 02  1.97E-10  2.20E-01
32  1.02E 01  1.94E 01 15.7-106 -26131H1  3.16E-10  8.02E 01   3.45E-09  2.32
  1.79E 02  1.97E-10  2.08E-01 -1.12E 01     898 278 23 32  1.02E 01  1.94E 0

123H1  2.85E-10  9.84E 01   1.67E-09  1.71E 00 -1.20E 00  3.00E-09  1.70E 02
2E 01     930 279  0 15  1.07E 01  1.97E 01 15.6-117 -28123L2  9.51E-11  0.0
  1.49E 00  5.09E-09  2.49E 02  1.14E-10  2.47E-01 -1.12E 01     931 279  0 1
.6-117 -28141L2  1.19E-10  0.0        4.27E-09  1.72E 00  3.02E-01  5.09E-09
2E-01 -1.12E 01     931 279  0 17  1.07E 01  1.97E 01 15.6-117 -28 83H3  2.19
  0.0        0.0        3.00E-09  0.0        1.87E-10  1.27E-01 -1.12E 01     94
.99E 01 15.5-123 -28123L2  1.45E-10  0.0        1.94E-09  1.57E 00  2.23E-01
7E-10  1.88E-01 -1.12E 01     947 279  0 39  1.10E 01  1.99E 01 15.5-123 -281
  4.55E-09  1.50E 00  8.25E-02  4.81E-09  2.90E 02  1.37E-10  1.73E-01 -1.12
.10E 01  1.99E 01 15.5-123 -28123H1  2.88E-10  6.54E 01   1.79E-09  1.53E 00
```

```
3E-01 -1.16E 01     522 278 14 59  1.10E 01  1
  1.75E 00  0.0        0.0        0.0          1.0
.61E 01 14.9  -8 -15 53H3  1.07E-09  1.49E 01
0E 00  4.15E-03 -1.15E 01     578 278 16 15  9
  0.0        0.0        0.0        0.0        0.0
.70E 00  1.64E 01 15.2 -17 -15123H1  3.15E-10
       1.00E 00  4.51E-02 -1.15E 01     642 27
  4.51E 01  0.0        0.0        0.0        3.0
8 18  4  9.10E 00  1.69E 01 15.6 -35 -16123H1
6E-09  1.87E 02  1.62E-10  1.54E-01 -1.14E 01
  1.66E-10  2.71E 03  3.13E-09  2.68E 00  3.1
    698 278 18 59  9.00E 00  1.73E 01 15.7 -4
7E-01  3.51E-09  1.60E 02  1.62E-10  1.70E-01
7 -17123L2  1.11E-10  0.0        1.86E-09  1.5
 -1.14E 01     699 278 19  0  9.00E 00  1.73E
3E 00  9.82E-02  5.06E-09  3.13E 02  1.07E-10
01 15.7 -47 -17 23H3  3.13E-10  3.06E 01  0.0
  0.0       -1.14E 01     714 278 19 21  9.00E
2E-09  1.58E 00 -1.52E 00  3.11E-09  1.83E 02
00  1.76E 01 15.8 -55 -19142H1  2.32E-10  1.2
  1.67E-10  2.13E-01 -1.14E 01     730 278 19
       2.27E-09  1.31E 00 -2.89E-01  4.56E-09
44  9.00E 00  1.76E 01 15.8 -56 -19

  4.56E-09  2.84E 02  1.60E-10  1.57E-01 -1.1  REC      4, LENGTH  2790
103H3  1.97E-10  1.25E 02  0.0        0.0
3E 01     746 278 20  4  9.00E 00  1.78E 01 15
  2.57E-01  4.74E-09  2.76E 02  1.16E-10  2.4
.9 -61 -19151L2  1.24E-10  0.0        4.51E-09
2E-01 -1.13E 01     747 278 20  6  9.00E 00  1
  2.45E 00  0.0        0.0        0.0        1.4
.79E 01 15.9 -65 -20123L2  1.43E-10  0.0
-E-10  1.43E-01 -1.13E 01     795 278 21 11  9
  4.43E-09  1.37E 00  3.99E-02  4.56E-09  2.8
.20E 00  1.82E 01 15.9 -75 -21123H1  2.69E-10
.E 02  1.39E-10  9.61E-02 -1.13E 01     834 27
  7.57E 01  3.28E-09  2.46E 00  1.69E-01  3.5
 22  4  9.50E 00  1.87E 01 15.9 -87 -23141H1
E-09  1.66E 02  1.39E-10  1.72E-01 -1.13E 01
  1.54E-10  0.0        1.87E-09  1.41E 00  1.3
    835 278 22  6  9.50E 00  1.87E 01 15.9 -8
-02  4.83E-09  3.05E 02  1.47E-10  1.21E-01
  -23123H1  3.19E-10  7.14E 01  1.87E-09  1.4
-1.12E 01     882 278 23 10  1.00E 01  1.92E
E 00  5.88E-02  3.70E-09  1.83E 02  1.90E-10
1 15.8-102 -26141H1  3.00E-10  9.00E 01  3.5
  1.52E-01 -1.12E 01     882 278 23 10  1.00E
E-09  1.46E 00 -1.27E 00  3.51E-09  2.15E 02
1  1.94E 01 15.7-106 -26122H1  3.17E-10  7.9
  1.97E-10  2.20E-01 -1.12E 01     898 278 23
E 01  3.45E-09  2.32E 00  1.59E-01  3.70E-09
2  1.02E 01  1.94E 01 15.7-106 -26

  3.00E-09  1.70E 02  2.11E-10  8.50E-02 -1.1  REC      5, LENGTH  2790
23L2  9.51E-11  0.0        1.57E-09  2.29E 00
E 01     931 279  0 17  1.07E 01  1.97E 01 15
  3.02E-01  5.09E-09  2.87E 02  1.14E-10  2.6
6-117 -28 83H3  2.19E-10  1.98E 02  0.0
E-01 -1.12E 01     946 279  0 37  1.10E 01  1
  1.57E 00  2.23E-01  4.51E-09  2.84E 02  1.3
99E 01 15.5-123 -28141L2  1.47E-10  0.0
-10  1.73E-01 -1.12E 01     947 279  0 39  1
  1.79E-09  1.53E 00 -1.41E 00  3.00E-09  1.8
```

```
0E 02  0.0        0.0        0.0        1.48E-09  0.0        1.10E-10  3.83E-02 -
11  3.22E 01  1.36E 01 10.8-102 -27133L2  6.01E-11  0.0        1.35E-09  1.75E
  2.45E 02  6.41E-11  1.51E-01 -1.93E 02  35223  94 10 12  3.15E 01  1.37E 01

151L2  6.33E-11  0.0        3.65E-09  1.51E 00  2.72E-01  4.37E-09  2.63E 02
3E 02  35223  94 10 12  3.15E 01  1.37E 01 10.9-103 -28143H1  1.80E-10  8.31E
 -1.51E 00  1.67E-09  9.19E 01  1.16E-10  8.30E-02 -1.93E 02  35238  94 10 33
.2-108 -28152H1  1.82E-10  1.48E 02  1.81E-09  2.83E 00  1.95E-01  1.94E-09
3E-01 -1.93E 02  35238  94 10 33  2.90E 01  1.42E 01 11.2-108 -28161H1  1.51E
  2.84E 00  2.09E-01  1.94E-09  8.54E 01  1.16E-10  1.85E-01 -1.93E 02  35238
.42E 01 11.2-108 -28 73H3  1.71E-10  6.87E 01  0.0        0.0        0.0
4E-10  4.95E-02 -1.93E 02  35254  94 10 55  2.69E 01  1.47E 01 11.5-112 -2811
  1.38E-09  2.16E 00  0.0        0.0        0.0        1.01E-10  1.45E-01 -1.93E
.47E 01  1.52E 01 11.9-117 -29 53H3  2.11E-10  4.15E 01  0.0        0.0
      1.02E-10  3.48E-02 -1.93E 02  35302  94 12  0  2.18E 01  1.62E 01 12.4
  6.22E 01  8.04E-10  1.86E 00 -6.67E-01  1.83E-09  9.95E 01  1.23E-10  1.81E
4 12 33  1.98E 01  1.69E 01 12.8-134 -30132H1  1.80E-10  8.87E 01  1.32E-09
3E-09  9.32E 01  1.23E-10  2.80E-01 -1.93E 02  35326  94 12 33  1.98E 01  1.6
  1.83E-10  8.57E 01  1.43E-09  2.73E 00  1.10E 00  2.13E-09  9.55E 01  1.23E
  35326  94 12 33  1.98E 01  1.69E 01 12.8-134 -30103L2  1.32E-10  0.0
      0.0        0.0        8.23E-11  2.89E-01 -1.93E 02  35327  94 12 34  1.9
4 -30 63H3  1.81E-10  6.97E 01  0.0        0.0        0.0        0.0        0.0
 -1.93E 02  35342  94 12 55  1.88E 01  1.73E 01 13.1-139 -30123H1  1.93E-10
4E 00  3.91E-01  1.23E-09  6.06E 01  1.21E-10  6.91E-02 -1.93E 02  35358  94
01 13.3-144 -30142H1  1.87E-10  8.18E 01  7.83E-10  2.80E 00  1.80E 00  1.49E
  1.00E-01 -1.93E 02  35358  94 13 16  1.80E 01  1.76E 01 13.3-144 -30161H1
2E-10  2.43E 00  1.14E 00  1.49E-09  7.06E 01  1.21E-10  2.40E-01 -1.93E 02
01  1.76E 01 13.3-144 -30 63H3  1.81E-10  6.97E 01  0.0        0.0        0.0
  1.01E-10  2.54E-02 -1.93E 02  35374  94 13 38  1.70E 01  1.81E 01 13.5-149
2E 01  0.0        0.0        0.0        9.54E-10  0.0        1.21E-10  3.88E-02
 0  1.63E 01  1.84E 01 13.7-154 -31 63H3  1.31E-10  2.49E 02  0.0        0.0
  0.0        1.14E-10  5.04E-02 -1.93E 02  35406  94 14 22  1.56E 01  1.86E 0

 73H1  2.10E-10  5.92E 01  4.40E-10  1.82E 00  1.03E-01  1.56E-09  8.57E 01
3E 02  35422  94 14 44  1.49E 01  1.89E 01 14.1-165 -30 82H1  2.14E-10  6.05E
  1.03E-01  0.0        8.57E 01  1.12E-10  3.61E-02 -1.93E 02  35422  94 14 4
.1-165 -30 23H3  2.53E-10  2.92E 01  0.0        0.0        0.0        0.0
      -1.93E 02  35438  94 15  5  1.43E 01  1.91E 01 14.3-170 -30143H1  1.86E
  1.77E 00 -1.34E 00  8.13E-10  4.52E 01  1.10E-10  9.45E-02 -1.93E 02  3545
.93E 01 14.5-176 -30152H1  1.65E-10  9.69E 01  7.66E-10  3.14E 00  5.11E-01
0E-10  1.68E-01 -1.93E 02  35454  94 15 27  1.37E 01  1.93E 01 14.5-176 -301
  7.55E-10  3.18E 00  5.64E-01  9.02E-10  3.75E 01  1.10E-10  1.61E-01 -1.93
.37E 01  1.93E 01 14.5-176 -30 83H3  1.66E-10  9.21E 01  0.0        0.0
      1.19E-10  4.28E-02 -1.93E 02  35470  94 15 49  1.33E 01  1.94E 01 14.
  7.80E 01  3.42E-10  2.86E 00  1.24E 00  1.13E-09  4.96E 01  1.13E-10  7.25
4 16 11  1.28E 01  1.94E 01 14.8 174 -29142H1  1.97E-10  7.14E 01  9.04E-10
      4.96E 01  1.13E-10  7.33E-02 -1.93E 02  35486  94 16 11  1.28E 01  1.
  1.81E-10  5.39E 01  0.0        0.0        0.0        7.97E-10  0.0        1.08
  35510  94 16 44  1.22E 01  1.94E 01 15.0 166 -29143H1  1.85E-10  7.84E 01
5E-02  1.56E-09  8.21E 01  1.16E-10  1.53E-01 -1.93E 02  35526  94 17  6  1.
1 -28152H1  1.72E-10  9.91E 01  1.02E-09  2.65E 00  1.85E 00  2.05E-09  9.33
 -1.93E 02  35526  94 17  6  1.18E 01  1.94E 01 15.1 161 -28161H1  1.84E-10
8E 00  9.85E-01  2.05E-09  1.03E 02  1.16E-10  1.95E-01 -1.93E 02  35526  94
01 15.1 161 -28123L2  6.73E-11  0.0        1.03E-09  1.52E 00  9.57E-01  4.23
  2.33E-01 -1.93E 02  35543  94 17 29  1.14E 01  1.92E 01 15.2 155 -27131L2
9E-09  1.30E 00  3.27E-01  4.23E-09  2.74E 02  6.63E-11  2.50E-01 -1.93E 02
01  1.92E 01 15.2 155 -27 83H3  1.73E-10  9.07E 01  0.0        0.0        0.0
  1.28E-10  3.49E-02 -1.93E 02  35560  94 17 38  1.12E 01  1.92E 01 15.2 152
0E 02  8.91E-10  2.07E 00 -1.42E-01  2.41E-09  1.24E 02  1.23E-10  1.08E-01
 0  1.09E 01  1.90E 01 15.3 147 -26103H3  1.59E-10  1.02E 03  0.0        0.0
  0.0        1.54E-10  6.25E-02 -1.93E 02  35582  94 18 22  1.06E 01  1.89E 0

123L2  1.17E-10  0.0        1.39E-09  1.64E 00  0.0        0.0        0.0
```

```
0E-10  3.83E-02 -1.93E 02  35222  94 10
  1.35E-09  1.75E 00  8.56E-01  4.37E-09
.15E 01  1.37E 01 10.9-103 -28

7E-09  2.63E 02  6.41E-11  2.02E-01 -1.9  REC    12. LENGTH  2790
  1.80E-10  8.31E 01  1.14E-09  1.81E 00
2  35238  94 10 33  2.90E 01  1.42E 01 11
5E-01  1.94E-09  8.55E 01  1.16E-10  1.9
8 -28161H1  1.51E-10  1.49E 02  1.81E-09
 -1.93E 02  35238  94 10 33  2.90E 01  1
      0.0        1.31E-09  0.0        1.1
01 11.5-112 -28113L2  1.01E-10  0.0
  1.45E-01 -1.93E 02  35271  94 11 18  2
      0.0        0.0        8.42E-10  0.0
01  1.62E 01 12.4-126 -29113H1  2.06E-10
  1.23E-10  1.81E-01 -1.93E 02  35326  9
7E 01  1.32E-09  2.86E 00  1.36E 00  2.1
33  1.98E 01  1.69E 01 12.8-134 -30151H1
9  9.55E 01  1.23E-10  3.81E-01 -1.93E 02
2E-10  0.0        3.75E-09  7.43E-01  0.0
327  94 12 34  1.98E 01  1.69E 01 12.8-13
  0.0        0.0        1.01E-10  2.54E-02
0123H1  1.93E-10  7.11E 01  3.87E-10  2.2
93E 02  35358  94 13 16  1.80E 01  1.76E
0  1.80E 00  1.49E-09  6.58E 01  1.21E-10
3.3-144 -30161H1  1.95E-10  7.48E 01  9.3
0E-01 -1.93E 02  35358  94 13 16  1.80E
  0.0        0.0        0.0        0.0
1.81E 01 13.5-149 -30 53H3  1.84E-10  7.9
1E-10  3.88E-02 -1.93E 02  35390  94 14
2  0.0        0.0        0.0        0.0
1.56E 01  1.86E 01 13.9-159 -31

6E-09  8.57E 01  1.12E-10  3.94E-02 -1.9  REC    13. LENGTH  2790
  2.14E-10  6.05E 01  1.36E-09  1.93E 00
2  35422  94 14 44  1.49E 01  1.89E 01 14
      0.0        0.0        1.00E 00  0.0
70 -30143H1  1.86E-10  6.98E 01  5.00E-10
2 -1.93E 02  35454  94 15 27  1.37E 01  1
4E 00  5.11E-01  9.02E-10  3.77E 01  1.1
01 14.5-176 -30161H1  1.64E-10  9.77E 01
  1.61E-01 -1.93E 02  35454  94 15 27  1
      0.0        0.0        7.66E-10  0.0
01  1.94E 01 14.6 179 -30133H1  1.83E-10
  1.13E-10  7.25E-02 -1.93E 02  35486  9
4E 01  9.04E-10  2.44E 00  1.24E 00  0.0
11  1.28E 01  1.94E 01 14.8 174 -29 73H3
  0.0        1.08E-10  4.96E-02 -1.93E 02
5E-10  7.84E 01  5.00E-10  1.97E 00  4.0
26  94 17  6  1.18E 01  1.94E 01 15.1 16
  2.05E-09  9.33E 01  1.16E-10  1.61E-01
161H1  1.84E-10  8.42E 01  1.32E-09  2.1
3E 02  35526  94 17  6  1.18E 01  1.94E
  9.57E-01  4.23E-09  2.54E 02  6.63E-11
.2 155 -27131L2  6.99E-11  0.0        3.2
0E-01 -1.93E 02  35543  94 17 29  1.14E
  0.0        0.0        1.05E-09  0.0
.92E 01 15.2 152 -27133H1  1.77E-10  1.0
3E-10  1.08E-01 -1.93E 02  35566  94 18
  0.0        0.0        0.0        1.48E-09
.06E 01  1.89E 01 15.4 143 -25

      0.0        1.10E-10  1.43E-01 -1.9  REC    14. LENGTH  2790
```

```
3E 02  35583  94 18 23  1.06E 01  1.88E 01 15.4 141 -25 63H3  1.89E-10  7.04E 01
  0.0        0.0        0.0        1.00E 00  3.10E-02 -1.93E 02  35598  94 18 44  1
.5 137 -24143H1  1.72E-10  1.02E 02  8.58E-10  1.98E 00 -5.94E-01  1.93E-09  1.0
5E-02 -1.93E 02  35614  94 19  6  1.00E 01  1.84E 01 15.6 132 -23152H1  1.60E-10
  2.37E 00 -5.94E-01  0.0        1.01E 02  1.21E-10  1.06E-01 -1.93E 02  35614  9
.84E 01 15.6 132 -23 93H3  3.00E-10  5.00E 01  0.0        0.0        0.0        1.3
1E-10  2.38E-01 -1.93E 02  35630  94 19 27  9.70E 00  1.82E 01 15.6 126 -22123L2
  1.40E-09  1.66E 00  0.0        0.0        0.0        1.08E-10  1.53E-01 -1.93E 02
.70E 00  1.82E 01 15.6 126 -22 63H3  2.02E-10  4.37E 01  0.0        0.0        0.0
       1.00E 00  4.29E-02 -1.93E 02  35646  94 19 49  9.50E 00  1.80E 01 15.7 12
  8.19E 01  5.24E-10  2.37E 00  8.97E-01  1.94E-09  9.30E 01  1.17E-10  1.09E-01
4 20 11  9.30E 00  1.78E 01 15.7 117 -20142H1  2.01E-10  7.56E 01  1.66E-09  2.0
       9.30E 01  1.17E-10  1.08E-01 -1.93E 02  35662  94 20 11  9.30E 00  1.78E
  1.27E-10  1.79E 02  0.0        0.0        0.0        7.45E-10  0.0        1.04E-10
  35678  94 20 33  9.10E 00  1.79E 01 15.7 111 -19 93H3  1.75E-10  5.40E 01  0.0
       7.85E-10  0.0        1.04E-10  3.33E-02 -1.93E 02  35694  94 20 55  8.90E
7 -17143L2  7.33E-11  0.0        8.27E-10  1.38E 00  4.06E-01  2.65E-09  1.67E 02
 -1.93E 02  35695  94 20 56  8.90E 00  1.73E 01 15.8 107 -17161L2  7.42E-11  0.0
7E 00  1.68E-01  2.65E-09  1.74E 02  7.33E-11  1.58E-01 -1.93E 02  35695  94 20
01 15.8 107 -17 43H3  1.48E-10  1.13E 02  0.0        0.0        0.0        0.0
  4.89E-02 -1.93E 02  35710  94 21 17  8.80E 00  1.71E 01 15.8 102 -16103H3  1.2
       0.0        0.0        7.88E-10  0.0        1.04E-10  6.29E-02 -1.93E 02  357
00  1.67E 01 15.8  92 -14 43H3  1.48E-10  1.13E 02  0.0        0.0        0.0
  1.04E-10  4.89E-02 -1.93E 02  35774  94 22 44  8.40E 00  1.63E 01 15.7  82 -11
0E 02  4.74E-10  2.35E 00 -9.34E-02  1.15E-09  5.50E 01  1.08E-10  1.16E-01 -1.9
27  8.30E 00  1.60E 01 15.6  72  -8162H1  1.32E-10  1.86E 02  8.15E-10  3.31E 00
  5.74E 01  1.08E-10  1.36E-01 -1.93E 02  35806  94 23 27  8.30E 00  1.60E 01 15
```

DAY 95 4/5/85

```
181H1  1.43E-10  1.36E 02  9.76E-10  2.83E 00  1.04E 00  1.41E-09  6.20E 01  1.0
3E 02  35806  94 23 27  8.30E 00  1.60E 01 15.6  72  -8103H3  1.51E-10  2.27E 02
  0.0        1.32E-09  0.0        1.30E-10  4.36E-02 -1.93E 02  35822  94 23 49  8
.6  68  -7133L2  9.01E-11  0.0        1.37E-09  1.52E 00  0.0        0.0        0.0
7E-02 -1.93E 02  35823  94 23 51  8.30E 00  1.58E 01 15.6  68  -7 93H3  1.78E-10
  0.0        0.0        9.83E-10  0.0        1.30E-10  6.31E-02 -1.93E 02  35838
.57E 01 15.5  64  -6 53H3  3.00E-10  5.00E 01  0.0        0.0        0.0        0.0
0E 00  4.29E-01 -1.93E 02  35854  95  0 33  8.40E 00  1.56E 01 15.5  58  -5133H1
  1.34E-09  1.70E 00  0.0        0.0        0.0        1.30E-10  6.34E-02 -1.93E 02
.50E 00  1.54E 01 15.4  54  -4
```

```
9E-10  7.09E 01  0.0        0.0
98  94 18 44  1.03E 01  1.87E 01 15
  1.93E-09  1.01E 02  1.21E-10  9.3
152H1  1.60E-10  1.35E 02  1.97E-09
3E 02  35614  94 19  5  1.00E 01  1
  0.0        1.38E-09  0.0        1.5
.6 126 -22123L2  1.16E-10  0.0
3E-01 -1.93E 02  35631  94 19 29  9
  0.0        0.0        0.0        0.0
.80E 01  5.7 122 -21133H1  1.88E-10
7E-10  1.09E-01 -1.93E 02  35662  9
  1.66E-09  2.07E 00  8.97E-01  0.0
.30E 00  1.78E 01 15.7 117 -20103H3
        1.04E-10  3.78E-02 -1.93E 02
  5.40E 01  0.0        0.0        0.0
4 20 55  8.90E 00  1.73E 01 15.8 10
6E-09  1.67E 02  7.33E-11  1.12E-01
  7.42E-11  0.0        2.33E-09  1.2
  35695  94 20 56  8.90E 00  1.73E
       0.0        0.0        1.09E-10
2 -16103H3  1.28E-10  1.60E 02  0.0
 -1.93E 02  35742  94 22  0  8.50E
       0.0        0.0        0.0
01 15.7  82 -11143H1  1.54E-10  1.0
  1.16E-01 -1.93E 02  35806  94 23
5E-10  3.31E 00  1.81E 00  1.41E-09
00  1.60E 01 15.6  72  -8

  6.20E 01  1.08E-10  1.85E-01 -1.9  REC    15. LENGTH   930
51E-10  2.27E 02  0.0        0.0
322  94 23 49  8.30E 00  1.58E 01 15
  0.0        0.0        8.84E-11  8.7
 93H3  1.78E-10  8.34E 01  0.0
93E 02  35838  95  0 11  8.40E 00  1
  0.0        0.0        0.0        1.0
5.5  58  -5133H1  1.96E-10  9.66E 01
34E-02 -1.93E 02  35870  95  0 55  8
```